ASTRONOMY & ASTROPHYSICS
SUPPLEMENT SERIES

Astron. Astrophys. Suppl. Ser. **120,** 489-520 (1996)

1.65 μm (H-band) surface photometry of disk galaxies. I. Observations of 158 galaxies with the Calar Alto 2.2 m telescope*,**

G. Gavazzi[1,2], D. Pierini[1,2], A. Boselli[3,4,5] and R. Tuffs[3]

[1] Università degli Studi di Milano, Via Celoria 16, 20133, Milano, Italy
[2] Osservatorio Astronomico di Brera, Via Brera 28, 20121 Milano, Italy
[3] MPI für Kernphysik, Postfach 103980, D-69117 Heidelberg, Germany
[4] DEMIRM, Observatoire de Paris, 61 Av. de l'Observatoire, 75014 Paris, France
[5] present address: Laboratoire d'Astronomie Spatiale, Traverse du Siphon, F-13376 Marseille Cedex 12, France

Received January 2; accepted May 7, 1996

Abstract. — Near Infrared (H-band) surface photometry of 158 (mostly) disk galaxies belonging to the Coma Supercluster and to the A262 and Cancer clusters was obtained using the 256^2 NICMOS3 array MAGIC attached to the 2.2 m Calar Alto telescope. Magnitudes and diameters within the 21.5 mag arcsec^{-2} isophote, concentration indices and total H magnitudes are derived.

Key words: galaxies: fundamental parameters — galaxies: photometry — infrared: galaxies

1. Introduction

The recent advent of large format near-infrared (NIR) detectors has made the study of the surface brightness distribution in galaxies at wavelengths longer than 1 μm relatively easy to obtain. Such new instruments, equipped with 256^2 arrays, provide for the first time the opportunity to study statistically significant samples of galaxies in the NIR (see e.g. de Jong & van der Kruit 1994).

The NIR wavelengths constitute the spectral region best adapted to study the quiescent stellar component of galaxies. As pointed out by Gavazzi (1993), the mass-to-light (M/L) ratio at 1.65 μm remains constant with galaxy mass, thus making the H-band luminosity an accurate indicator of the system luminous mass. Moreover, within a galaxy, the NIR bands trace mass better than do optical bands, as they are less contaminated by the low M/L products of recent episodes of star formation. The NIR spectral region provides yet another advantage: the internal extinction at 1.65 μm is more than seven times lower than in the B band (e.g. Landini et al. 1984).On the other side, the sky brightness can be as much as ten magnitudes brighter than in the visible; thus more sophisticated and time-consuming observing and data reduction techniques are required.

In this paper, we present 1.65 μm (H-band) surface brightness measurements of 158 galaxies selected among the members of the A262, Cancer, Coma and A1367 clusters (primarily of late-type, but some E and S0s are included). In addition, we selected a significant population of galaxies in the portion of the "Great Wall" which lies in the bridge between Coma and A1367. These objects are treated as isolated and will be used as a control sample for environmental studies.

The observations were obtained with the MAGIC NIR camera mounted on the 2.2 m Calar Alto telescope. By themselves the 158 observations reported in this paper are not complete in any statistical sense. However, together with the observations of 297 galaxies described in a companion paper of this series (Gavazzi et al. 1996a) (Paper II), carried out with the TIRGO 1.5 m telescope, these measurements comprise a complete sample of spiral/Irr galaxies, at least in the region of the Coma supercluster. The coverage of the A262 and Cancer clusters is less complete: to date we observed 41/62 spirals in A262 and 29/37 in the Cancer cluster.

Send offprint requests to: G. Gavazzi

*based on observations taken at the Calar Alto Observatory, operated by the Max Planck Institut für Astronomie (Heidelberg) jointly with the Spanish National Commission for Astronomy

**Tables 1 and 2 are only available in electronic form at the CDS via anonymous ftp to cdsarc.u-strasbg.fr (130.79.128.5) or via http://cdsweb.u-strasbg.fr/Abstract.html

For the combined sample, we also have extensive auxiliary data available, namely optical (B, V) images (Gavazzi et al. 1990; Gavazzi & Randone 1994b; Gavazzi et al. 1994a; Gavazzi et al. 1995a) and high signal-to-noise H I spectra acquired at Arecibo (Gavazzi 1987, 1989 and references therein).

A third NIR observational study is focused on the Virgo cluster (Boselli et al. 1996), in particular on the subsample of late-type Virgo galaxies included in the ISO core-program.

The data were collected with the primary aim of determining redshift-independent distances using the Tully-Fisher (TF) relation (Tully & Fisher 1977) and total H magnitudes, obtained by extrapolating the available measurements to the radius corresponding to the optical diameter (as explained in Gavazzi & Boselli 1996). These total magnitudes, determined from two-dimensional observations, should be significantly more accurate than previous determinations based on aperture photometry measurements (e.g. Aaronson et al. 1986; Gavazzi et al. 1991) since they are obtained with less growth-curve extrapolation and don't suffer from contamination from stars in the field.

In this paper we report on the observations collected and analyzed to date with the Calar Alto instrumentation. Section 2 describes the sample studied, and the observations are outlined in Sect. 3. Image analysis strategies are discussed in Sect. 4.

The analysis of the present observations is postponed to Paper II, joined with similar observations obtained with the TIRGO instrumentation.

Other issues, including the comparison between NIR and optical properties, the mass-to-light ratio in galaxies, which has direct implications on galaxy dark matter content, are addressed in Gavazzi et al. (1996).

2. Sample selection

The galaxies observed in this work are selected from the CGCG catalogue (Zwicky et al. 1961-1968), thus with $m_p \leq 15.7$, in 2×2 deg^2 regions containing the A262 and Cancer clusters and in the Coma supercluster region $11.5^h \leq \alpha \leq 13.5^h$; $18° \leq \delta \leq 32°$ including the Coma and A1367 clusters. More informations on the selection criteria in the surveyed regions can be found in Gavazzi & Boselli (1996). In these regions we observed primarily spiral galaxies with type later than Sa. Even in this morphological class the present observations do not form a complete sample; however, in conjunction with the objects observed at TIRGO (Paper II) the coverage of the survey is as follows: in A262 we imaged 41 objects out of 62 spirals; 29 out of 37 in the Cancer cluster. Out of the 507 spiral galaxies projected onto the region of the Coma supercluster, we observed 257. However limited to the Coma supercluster members (i.e. with velocities in the range: $5000 < V < 8000$ km s^{-1}, see Gavazzi et al. (1995b) for details on supercluster membership and for the separation between cluster and field samples) the fraction of galaxies observed is 245/279. If, among these, we consider only the 221 spirals with $m_p \leq 15.6$, we observed 209; thus, to this limiting magnitude this subsample can be considered complete.

The observations of the Virgo cluster region carried out at Calar Alto in the K' band with an observing strategy similar to the one described in this paper and in Paper II are reported in Boselli et al. (1996).

Table 1 lists the relevant parameters of the galaxies observed in this work. The table is arranged as follows:
Column 1: CGCG denominations (Zwicky et al. 1961-68). Few galaxies, fainter than the CGCG limit are taken from Butcher & Oemler (1985). Two faint objects in A1367 (#3 and #4) are from Gavazzi & Contursi (1994).
Columns 2, 3: adopted (1950) celestial coordinates.
Column 4: "aggregation" parameter. This parameter defines the membership to a group/cluster/supercluster: CSisol, CSpairs, CSgroups indicate members of the Coma Supercluster ($5000 < V < 8000$ km s^{-1}); CSforeg means objects in the foreground of the Coma Supercluster ($V < 5000$ km s^{-1}) and CSbackg means objects in the background of the Coma Supercluster ($V > 8000$ km s^{-1}).
Column 5: morphological type.
Columns 6, 7: major and minor optical diameters (in arcmin) derived as explained in Gavazzi & Boselli (1996). These diameters are consistent with those given in the RC3.
Column 8: CGCG photographic magnitude.
Column 9: total H magnitude (H_T) obtained extrapolating the present photometric measurements (combined with those of Paper II) to the optical diameter along circular apertures, corrected for internal extinction as outlined in Gavazzi & Boselli (1996).
Column 10: observing year.

3. Observations and image reduction

The observations reported in this paper were carried out in February 1994 and 1995 with the 2.2 m telescope at Calar Alto. Out of the 13 scheduled nights, 6 were useful and only 3 entirely photometric.

The folded Cassegrain focus of the telescope was equipped with the MAGIC NIR camera, which relies on a 256^2 NICMOS3 array detector (Herbst et al. 1993). Since these observations were planned as a side-product of a survey of Virgo galaxies, containing targets with large apparent size, the optical set-up of the detector was the one chosen to give the largest possible field of view, i.e. 6.8×6.8 arcmin^2, with a pixel size of 1.61 arcsec. In one night of 1995 (Feb-15) we used a different optical set-up with a pixel size of 0.64 arcsec and a corresponding field of view of 2.7×2.7 arcmin^2.
All observations were obtained with a seeing typically of

1-2 arcsec.
Obtaining a satisfactory background subtraction is the challenge of IR observations. At 1.65 μm the sky brightness at Calar Alto is tipically 13.8 mag arcsec^{-2} and it is variable on time scales comparable with the duration of an observation (Wainscoat & Cowie 1992). To reach a brightness limit 8−9 mag arcsec^{-2} fainter than the sky requires an image in which the deviations from flatness are less than 0.05%. Thus, data acquisition techniques must involve the monitoring of the sky fluctuations and data reduction must take account of them.

For this reason, two types of pointing sequences (or "mosaics") were programmed, according to the galaxy sizes (see Fig. 2 in Boselli et al. 1996). Galaxies with optical diameter larger than 3.5 arcmin were observed using a mosaic in which 50% of the time is devoted to the target of interest and 50% to the surrounding sky (hereafter denoted as a type "A" mosaic). This pattern was obtained alternating eight fields centered on the target with eight observations of the sky, chosen along a circular path around the galaxy (off-set by 7 arcmin from the center). The eight on-target fields were dithered by 10 arcsec in order to facilitate bad pixel removal.
To save telescope time, galaxies with optical diameter smaller than 3.5 arcmin were observed with a mosaic constituted of nine pointings along a circular path and displaced one another by 2 arcmin such that the target galaxy is always in the field (hereafter denoted as type "B" mosaic). On-chip integration times were set to avoid saturation but to ensure background-limited performance. Several short elementary integrations of 3−5 s were added by the on-line acquisition software during each pointing to give total integration times on-source of 300 s or more.

3.1. *Photometric calibration*

The observations were calibrated using the standard stars: HD 40335 (H=6.47 mag), HD 84800 (H=7.53 mag) and HD 129653 (H=6.92 mag) taken from Elias et al. (1982), which were observed hourly throughout the night. The calibration stars were observed with a third mosaic (type "C"), wich consists of five positions, starting with the star near to the center of the array, followed by positioning the star in each of the four quadrant. The telescope was defocused to avoid saturation.
After image reduction (see below) and after performing virtual aperture photometry, the typical uncertainty in the calibration during photometric periods is 0.05 mag.

3.2. *Data reduction procedures*

The multiplicative correction for the system response (usually named flat-field) was determined daily taking exposures of the telescope dome with and without illumination from a quartz lamp. We used as the flat-field (FF) frame the image difference of the two exposures, normalized to its mean. Specific reduction strategies were used for the various mosaics. For type "A" mosaics the (usually eight) sky exposures were combined with a median algorithm to form a median sky. For type "B" and "C" mosaic, the median sky was determined combining all the frames in the pointing sequence whose mean counts differed from the mean by less than 5%. In unstable conditions of the sky (variations larger than 5% over the whole pointing sequence), the use of such a median sky would introduce low-frequency gradients in the final combined image, because of spatial variations of the sky. In this case, a median sky was obtained by combining the three closest in time images of the sky (type "A" mosaic) or of target+sky (type "B" and "C" mosaic). The median algorithm is necessary to remove contaminating star and galaxy images in the median sky frames. The median sky was first normalized to its average counts, then multiplied by the average counts of the individual target frames; finally this riscaled frame was subtracted from each of the target observations. Such a procedure accounts for temporal variations in the sky level which are of the order of 5% during a pointing sequence, but introduces an additive offset which is subsequently removed (see below).

The sky subtracted target frames were then divided by the FF frame. Each of these corrected frame was then inspected for low-spatial-frequency gradients, and, if necessary, fitted with a two-dimensional 3 to 5 degree polynomial which was then subtracted. If this process failed, the corresponding frames were rejected from further analysis. Finally, the corrected frames were registered using field stars and combined with a median filter (which allowed bad pixel removal). Foreground stars were manually edited from the images. All image reduction and data analysis was performed in the IRAF environment and relied on the STSDAS package.[1]

We have assessed the quality of the final images both on small spatial scales, and over the entire array, and the flatness of the FF frames, over an entire raw or column and on few pixels scale. The images are truly background limited: on small scale the noise is consistent with the expected statistical fluctuations in the photon counts of the background. On the large scale (comparable with the size of the measured objects) the deviation from flatness is <0.05% − 0.08% of the background in photometric and non-photometric conditions respectively (corresponding to ∼22.0 mag arcsec^{-2}), i.e. ∼10% of the individual

[1]IRAF is the Image Analysis and Reduction Facility made available to the astronomical community by the National Optical Astronomy Observatories, which are operated by AURA, Inc., under contract with the U.S. National Science Foundation. STSDAS is distributed by the Space Telescope Science Institute, which is operated by the Association of Universities for Research in Astronomy (AURA), Inc., under NASA contract NAS 5–26555.

pixel noise σ, representing the major source of error in low S/N regions.

4. Image analysis

4.1. *Virtual aperture photometry*

At the position of each galaxy center a growth curve was derived by integrating the counts in concentric circular rings of increasing radii. The sky value was determined in a concentric object-free corona (where average sigma-clipping takes care of rejecting the contribution from contaminating stars).

4.2. *A posteriori photometric calibration*

By the zero-points determined from standar star calibration, it was possible to transform the resulting H-band growth curves from counts to magnitudes. A comparison of the magnitudes, obtained before the removal of foreground stars from the frame, with multiaperture photometry available in the literature (usually uncorrected for star contamination) was successively made. It provided a check on the standard star calibration and a way to correct the photometric calibration for all galaxies observed under partially photometric conditions. If we compare our "virtual aperture" measurements with the 270 aperture photometry measurements available from the literature, taken through apertures consistent within 0.5 arcsec from ours, we find that the two sets of measurements are consistent in the average, with 0.09 mag scatter. The most discrepant measurements are those at small apertures (5−15 arcsec), due to a combination of seeing effects and unaccurate galaxy centering. We estimate that the overall photometric accuracy of our data (including systematic errors on the zero point determination) is ≤ 0.1 mag.

4.3. *Total H-band magnitudes*

Total H-band magnitudes given in Table 1 are obtained according to Gavazzi & Boselli (1996). These are magnitudes extrapolated along circular apertures to the optical diameter (a_{25}), corrected for internal extinction using $\Delta m_i = -2.5D \log(b/a)$, where D=0.17, as determined in Boselli & Gavazzi (1994). For 19 objects in common with Paper II the total magnitudes are obtained combining the two data-sets.

4.4. *Elliptically extracted profiles*

Using the star-subtracted frames, the surface brightness profiles were re-determined by averaging the light distribution in concentric elliptical annuli of fixed center, position angle and ellipticity. The position angles and ellipticities were determined by eye fitting the 21 H-mag arcsec^{-2} isophotes of the galaxies under study. This rather simple and often not accurate procedure was preferred to more sophisticated techniques (such as those with variable center, position angle and ellipticity) because, in any case, for spiral and irregular galaxies ellipses are just crude representations of their morphology, and for consistency with the method adopted in optical CCD studies (see Gavazzi et al. 1995a and references therein). Starting from an inner ellipse of size comparable with the seeing disk, a set of annuli was derived, by increasing the major axis linearly by fixed amounts. For each ring the total number of counts and the area in pixels were calculated. The statistical uncertainties on the net counts in each annulus were computed as in Gavazzi et al. (1994a). Figure 1 shows in the left-hand panel grey-scale/contour representations of the galaxies presented in this paper. The faintest contour level shown is 20.5 mag arcsec^{-2} with steps of 0.5 mag arcsec^{-2}. The right-end panel of Fig. 1 presents the H-band surface brightness profile in mag arcsec^{-2} as described above. The horizontal scale gives the radius in arcsec as measured from the galaxy center along the semi-major axis of the ellipse.

4.5. *Isophotal radii, magnitudes, and concentration indices*

H-band isophotal major radii ($a_{21.5}$) are determined in the azimuthally integrated profiles as the radii at which the surface brightness reaches 21.5 H-mag arcsec^{-2}. The values of $a_{21.5}$ given in this work are not corrected for galaxy inclination.

H-band magnitudes ($H_{21.5}$) are derived by integrating the elliptical light profiles up to $a_{21.5}$. Again, these magnitudes are measured quantities and are not corrected to the face-on value. As in earlier papers (Gavazzi et al. 1990; Gavazzi et al. 1994a), we have also derived a model-independent concentration index, similar to that defined in de Vaucouleurs (1977). This is the ratio between the radii that enclose 25% and 75% of the isophotal magnitude, ($H_{21.5}$). Table 2 summarizes these measured photometric parameters for the galaxies presented in this paper.

Column 1: CGCG denomination;

Column 2: observing dates (day-month-year);

Column 3: pixel size in arcsec.

Column 4: Total integration time (in seconds) written as the product of the number of coadds N_c, the on-chip integration time t_{int}, and the number of frames N_f combined to form the final image. Some galaxies ($N_f = 1$) were serendipitously observed in the sky frames of other targets.

Column 5: Photometric quality: galaxies marked * were observed in non-photometric periods and their zero point is derived from the reference aperture photometry;

Column 6: Position Angle of the galaxy major axis (measured counterclockwise from N);

Column 7: ellipticity ($1 - b/a$) of the elliptical rings used to derive the surface brightness profiles;

Column 8: galaxy observed major ($a_{21.5}$) radius (in arcsec) determined at the 21.5$^{\rm th}$ magnitude isophote;
Column 9: observed magnitudes ($H_{21.5}$) integrated within the 21.5 mag arcsec^{-2}elliptical isophote;
Column 10: concentration index c_{31}, as defined in Gavazzi et al. (1990), is the ratio between the radii that contain 25% and 75% of $H_{21.5}$.
Nineteen galaxies in the present investigation were reobserved at TIRGO (see Paper II). The rms scatter between the two sets of measurements is 0.20 mag, larger than expected. However 6 of these objects were taken serendipitously in some sky measurements of other target objects, thus with a noise higher than average. If we exclude these 6 objects the discrepancy reduces to 0.13 mag (1σ).

5. Conclusions and Summary

Using the Calar Alto 2.2 m telescope equipped with the MAGIC NIR camera we obtained images in the near-infrared H band for 158 nearby ($z < 0.02$) galaxies chosen from a magnitude selected ($m_{\rm p} \leq 15.7$) sample. As mentioned in the introduction, the galaxies presented in this paper do not form a complete sample. Therefore the NIR properties of the present subsample are analyzed in Paper II in conjunction with the observations taken similarly at TIRGO.

Here we wish only to anticipate that the results of the present investigation are in full agreement with the ones obtained for the TIRGO subsample of 297 objects, namely:
1) The H-band light profiles of spiral galaxies have generally the shape typical of exponential disks. Relevant bulges are mainly found among luminous (massive) objects with $M_H < -22$.
2) The H band isophotal radii at the 21.5 mag arcsec^{-2} are 20% smaller than the corresponding B band radii determined at the 25 mag arcsec^{-2} isophote.
3) The concentration index, i.e. the ratio between the radii that enclose 25% and 75% of the isophotal magnitude, $H_{21.5}$, is primarily related to the H luminosity, rather than to the morphological type of galaxies. Luminous objects are more centrally concentrated than faint ones.

Acknowledgements. We thank the MAGIC team at MPI für Astronomie for their skilful operational support and for several helpful discussions about data reduction. We thank Bianca Garilli for writing some useful IRAF procedures. A.B. is supported through the Verbundforschung Astronomie/Astrophysik of DARA, under grant # 50-OR-95018).

References

Aaronson M., et al., 1986, ApJ 302, 536
Boselli A., Gavazzi G., 1994, A&A 283, 12
Boselli A., Tuffs R., Gavazzi G., Hippelein H., Pierini D., 1996, A&AS (in press)
Butcher H., Oemler A., 1985, ApJS 57, 665
de Jong R., van der Kruit P., 1994, A&AS 106, 451
de Vaucouleurs G., 1977, in "Evolution of Galaxies and Stellar Populations". In: Larson R. & Tinsley B. (eds.), New Haven: Yale University Observatory, p. 43
Elias J.H., Frogel J.A., Matthews K., Neugebauer G., 1982, AJ 87, 1029
Gavazzi G., 1987, ApJ 320, 96
Gavazzi G., 1989, ApJ 346, 59
Gavazzi G., Garilli B., Boselli A., 1990, A&AS 83, 399
Gavazzi G., Scodeggio M., Boselli A., Trinchieri G., 1991, ApJ 382, 19
Gavazzi G., 1993, ApJ 419, 469
Gavazzi G., Contursi A., 1994, AJ 108, 24
Gavazzi G., Garilli B., Carrasco L., Boselli A., Cruz Gonzalez I., 1994a, A&AS 104, 271
Gavazzi G., Randone I., 1994b, A&AS 107, 285
Gavazzi G., Boselli A., Carrasco L., 1995a, A&AS 112, 257
Gavazzi G., Randone I., Branchini E., 1995b, ApJ 438, 590
Gavazzi G., Boselli A., 1996, Ap. Lett. Comm. 35, 1
Gavazzi G., Pierini D., Baffa C., Lisi F., Hunt L., Randone I., Boselli A., 1996a, A&AS 120, 521 (Paper II)
Gavazzi G., Pierini D., Boselli A., 1996, A&A 312, 397
Herbst T., Beckwith S., Birk C., et al., 1993, SPIE 1946
Landini M., Natta A., Salinari P., Oliva E., Moorwood A., 1984, A&A 134, 284
Tully B., Fisher J., 1977, A&A 54, 661
Wainscoat R., Cowie L., 1992, AJ 103, 332
Zwicky F., et al., 1961-1968, "Catalogue of Galaxies and Clusters of Galaxies", Vol. 6, Pasadena, C.I.T.

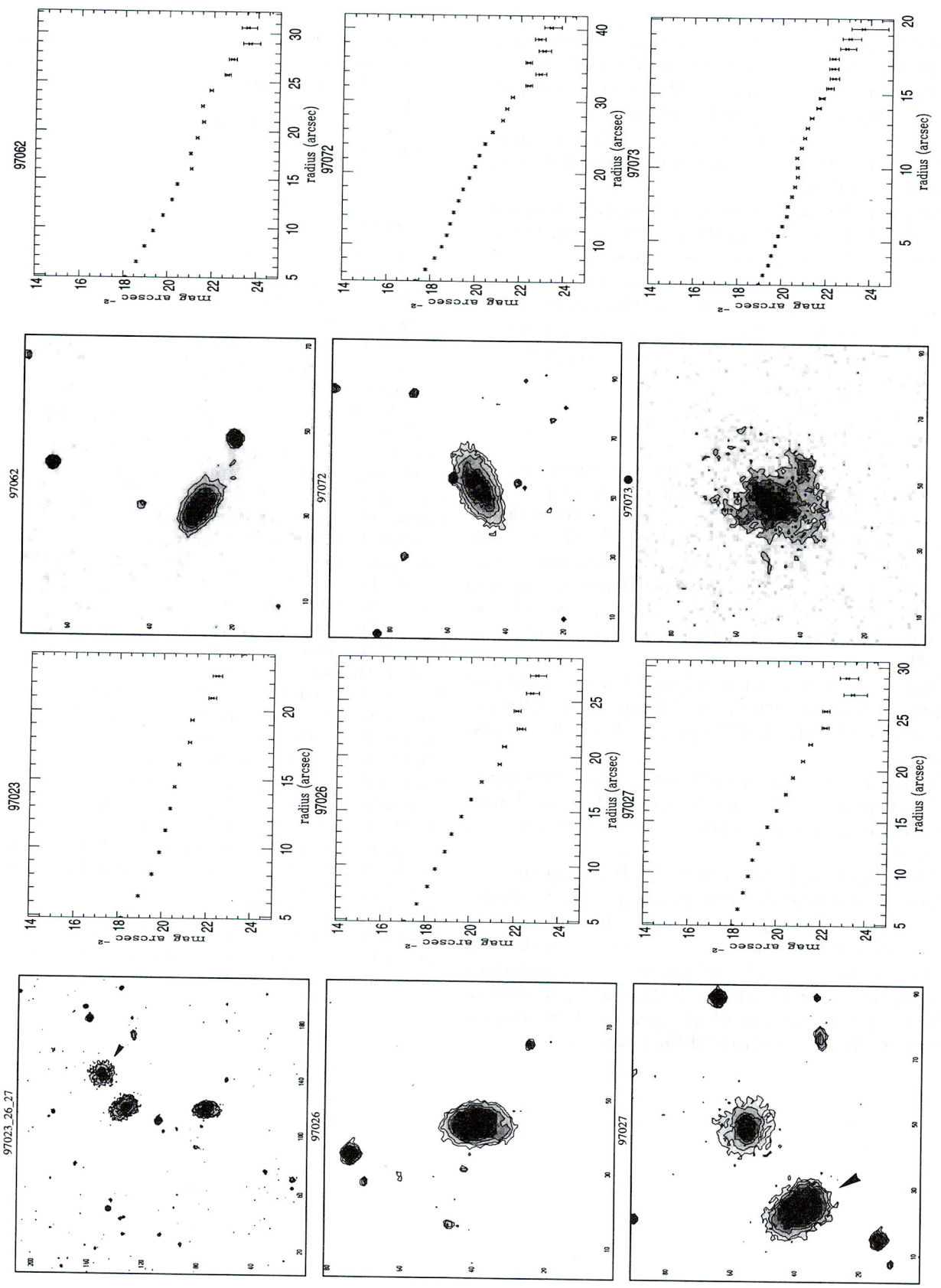

Fig. 1. Grey–level/contour representations of the H band frames of galaxies under study (left panels). N is up, E to the left. The faintest contour level shown is 20.5 mag arcsec^{-2}; the grey scale is arbitrary. The angular scale of the images can be derived from the labels around the frames (1 pixel = 1.61 arcsec, otherwise 0.64 arcsec, as marked with a dot near the figure label). H band radial surface brightness profiles of the galaxies under study obtained along elliptical annuli (right panels). **(To be seen in landscape)**

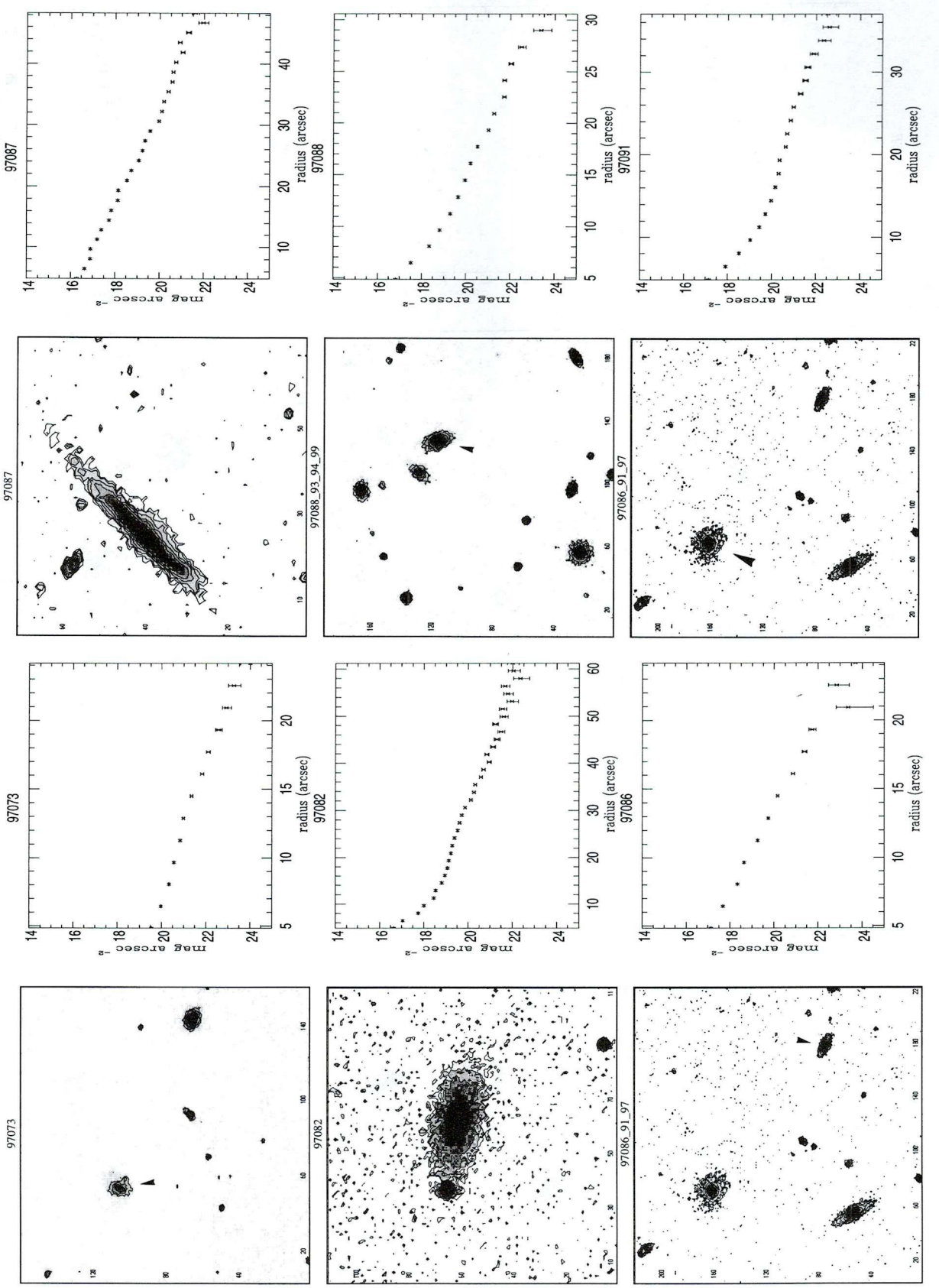

Fig. 1. continued. **(To be seen in landscape)**

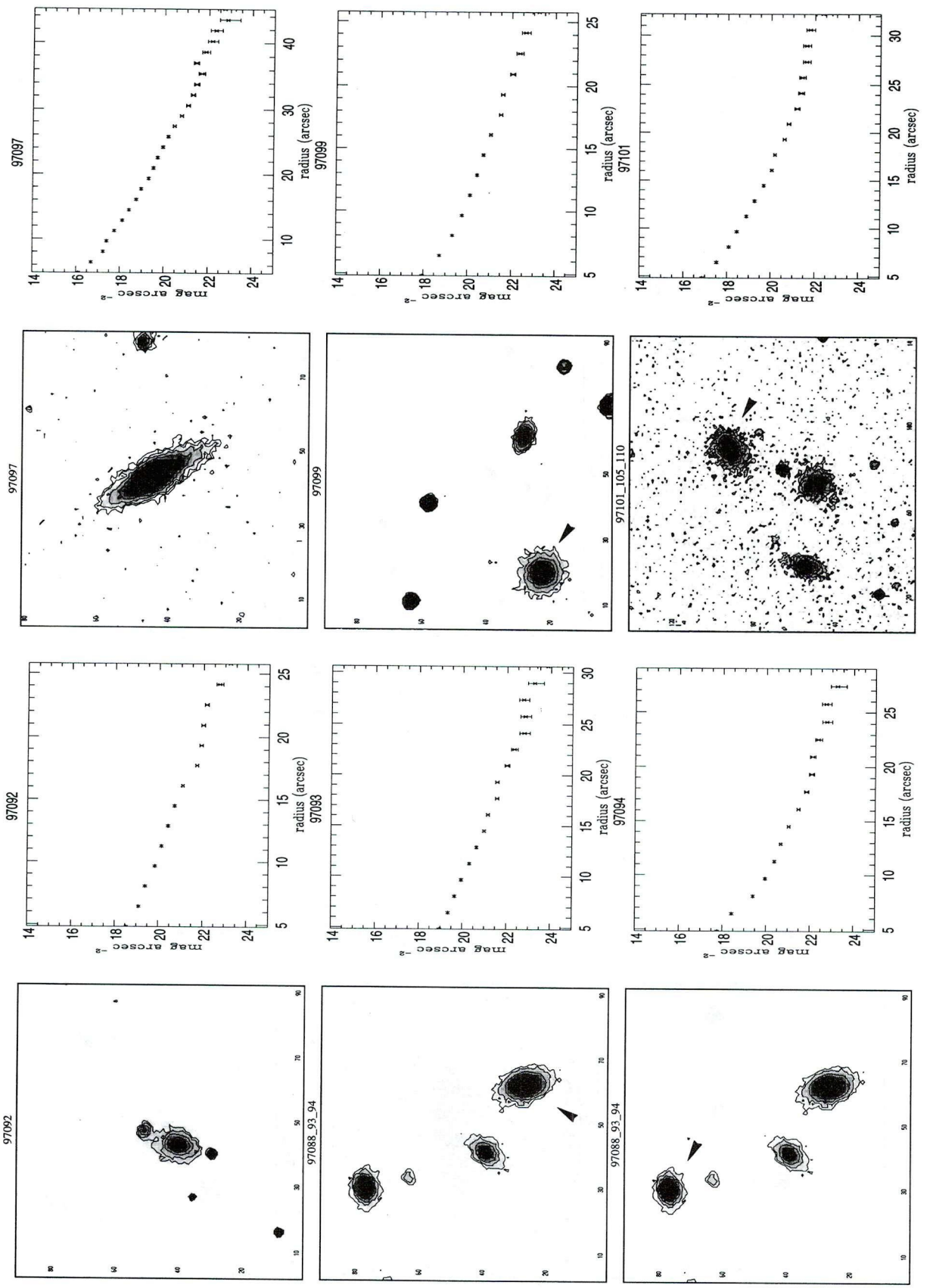

Fig. 1. continued. **(To be seen in landscape)**

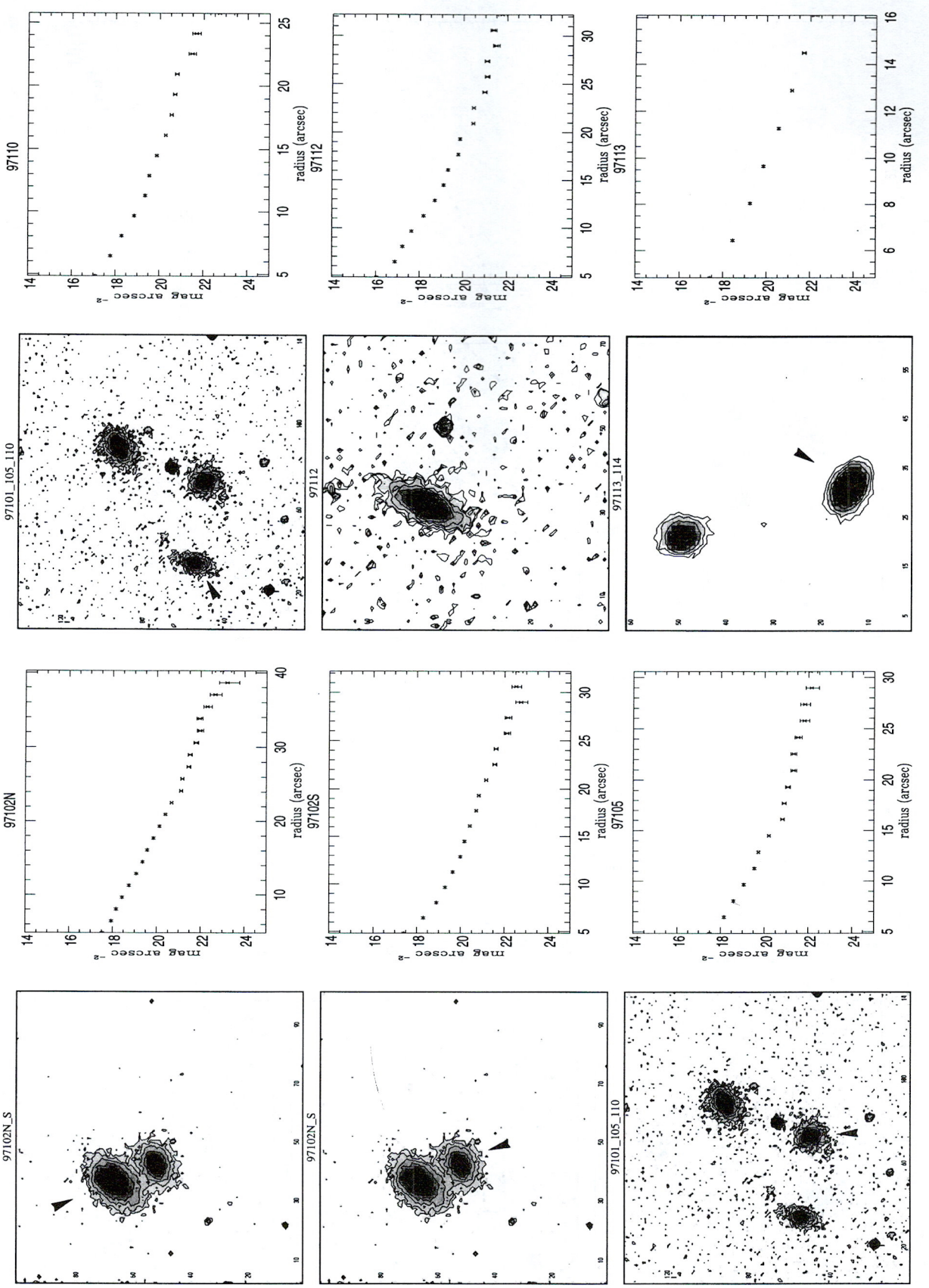

Fig. 1. continued. **(To be seen in landscape)**

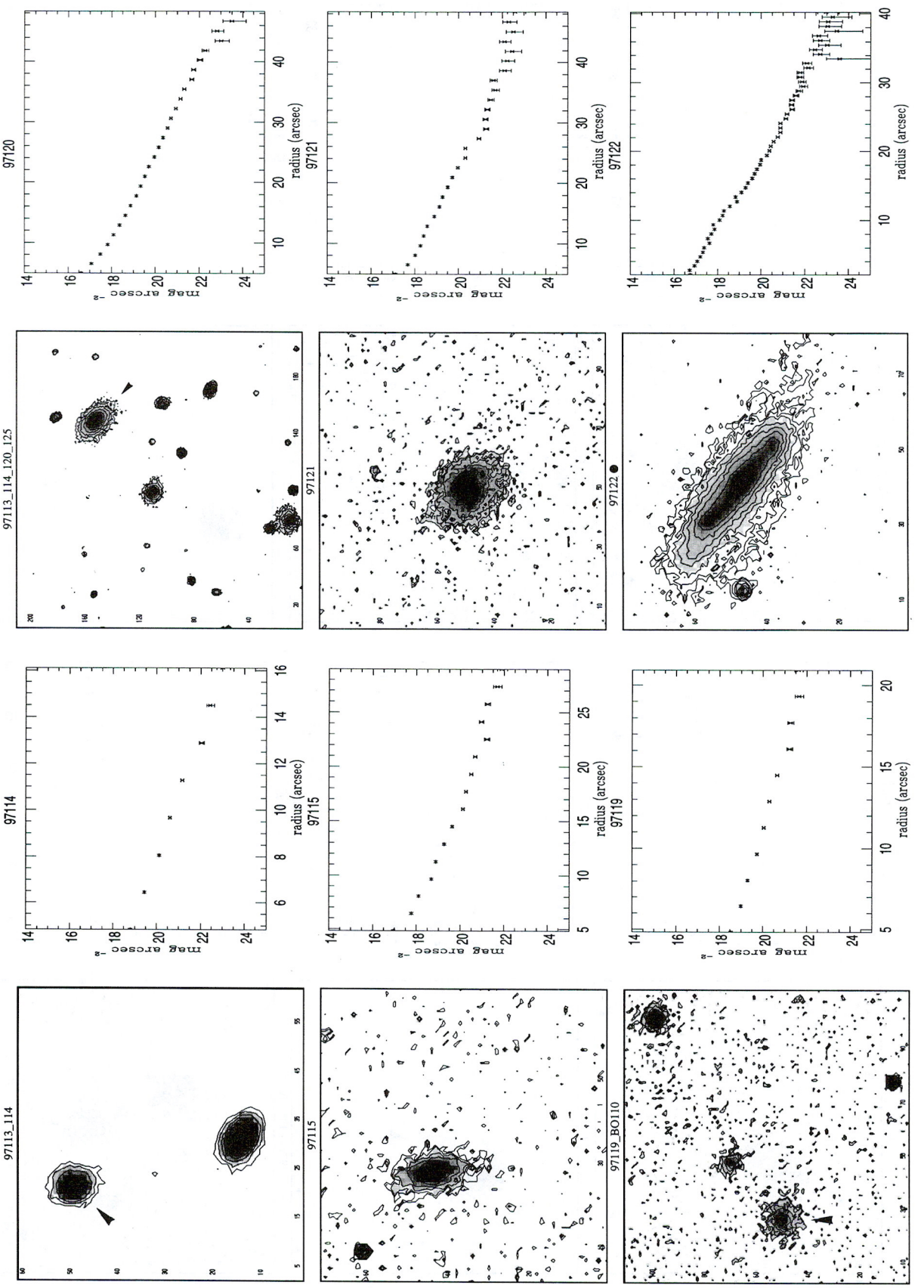

Fig. 1. continued. **(To be seen in landscape)**

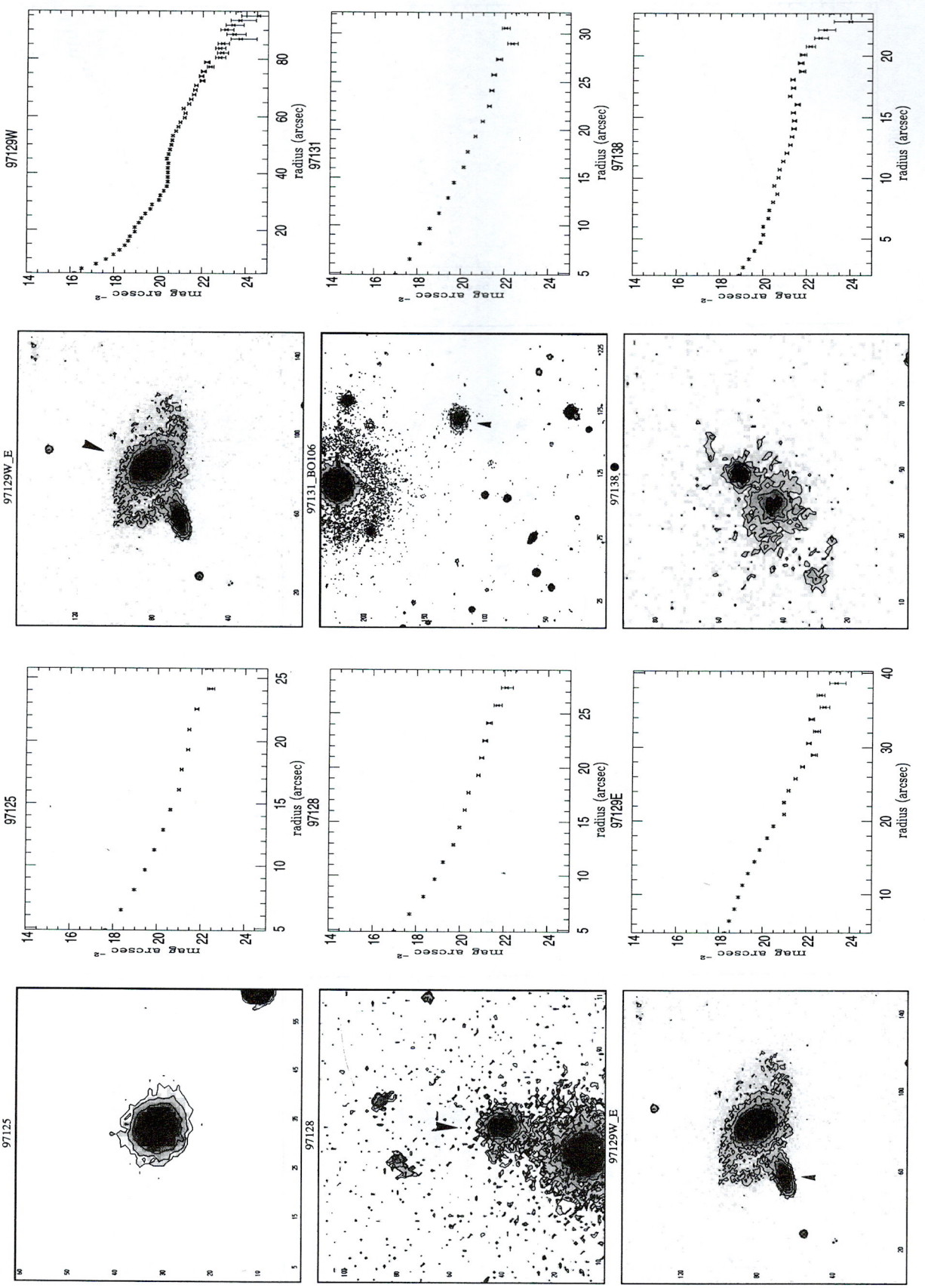

Fig. 1. continued. **(To be seen in landscape)**

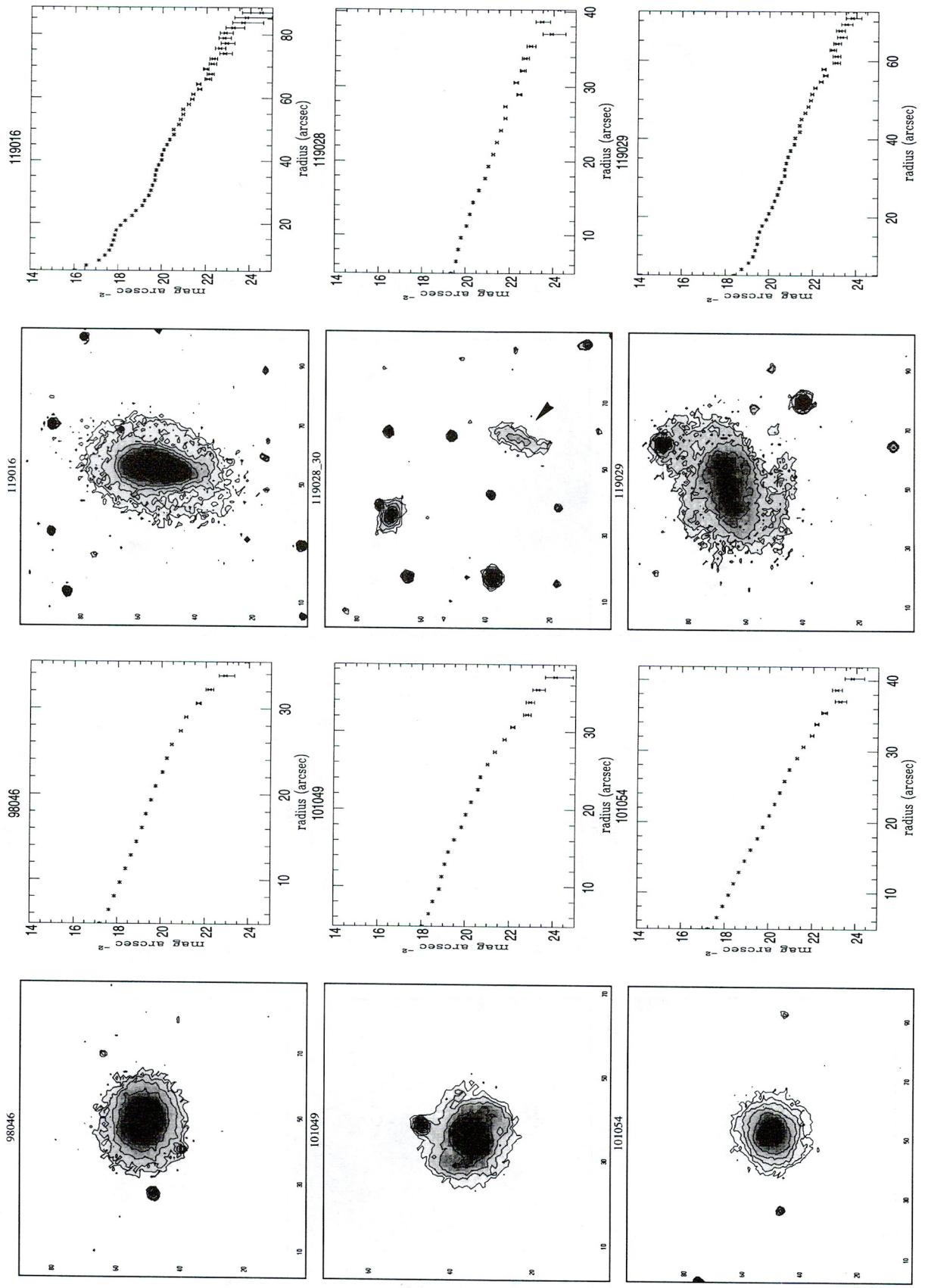

Fig. 1. continued. **(To be seen in landscape)**

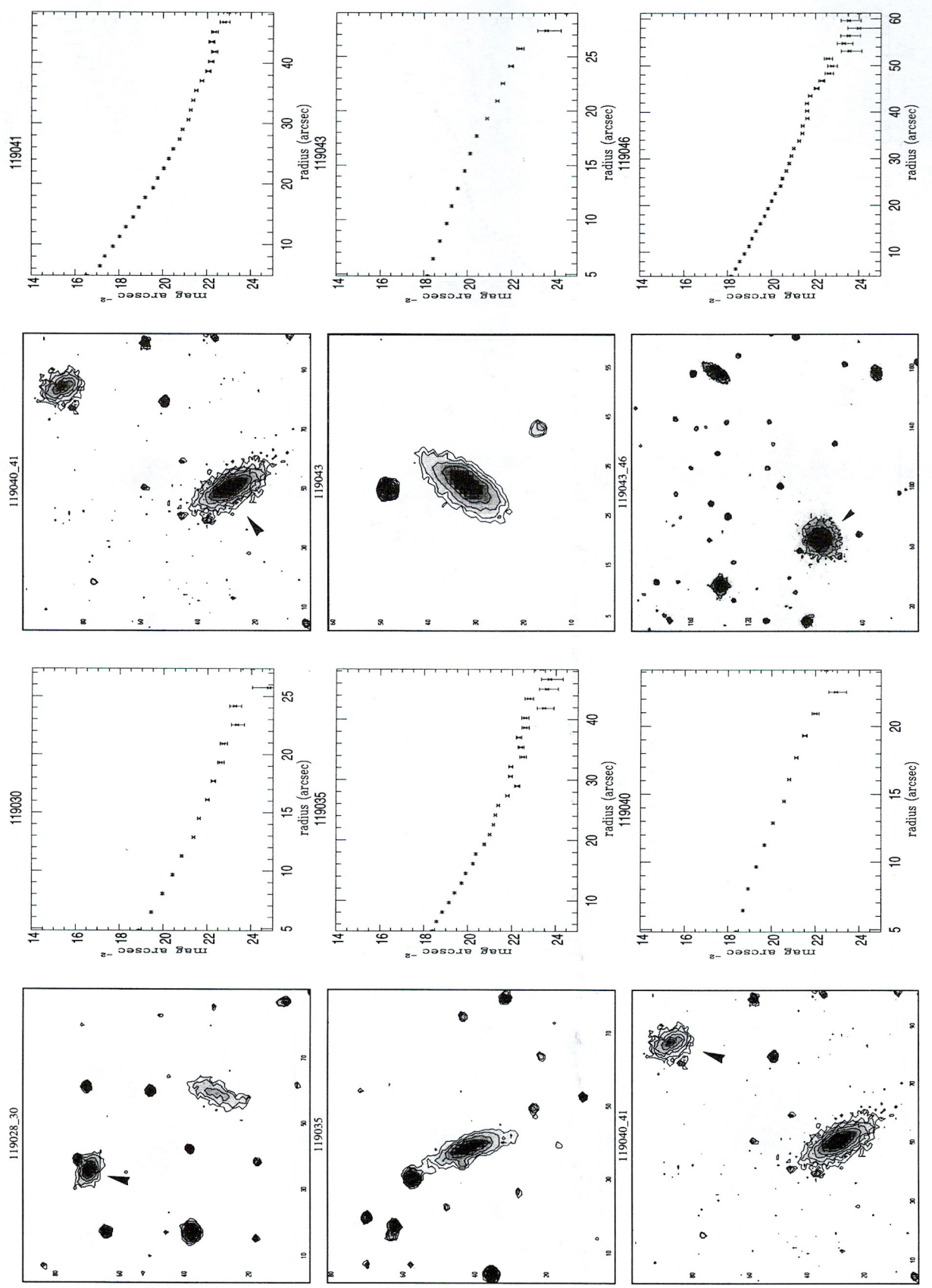

Fig. 1. continued. **(To be seen in landscape)**

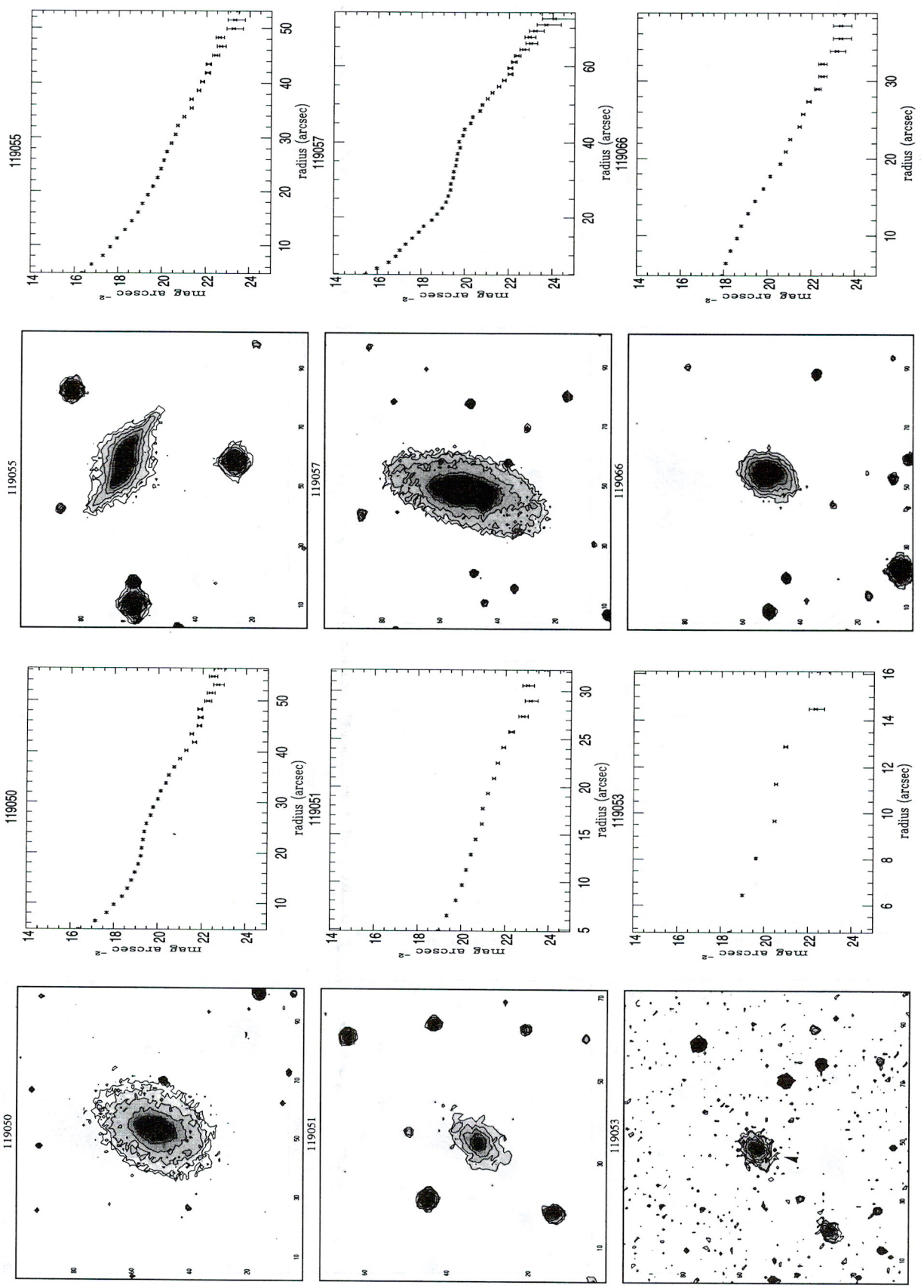

Fig. 1. continued. **(To be seen in landscape)**

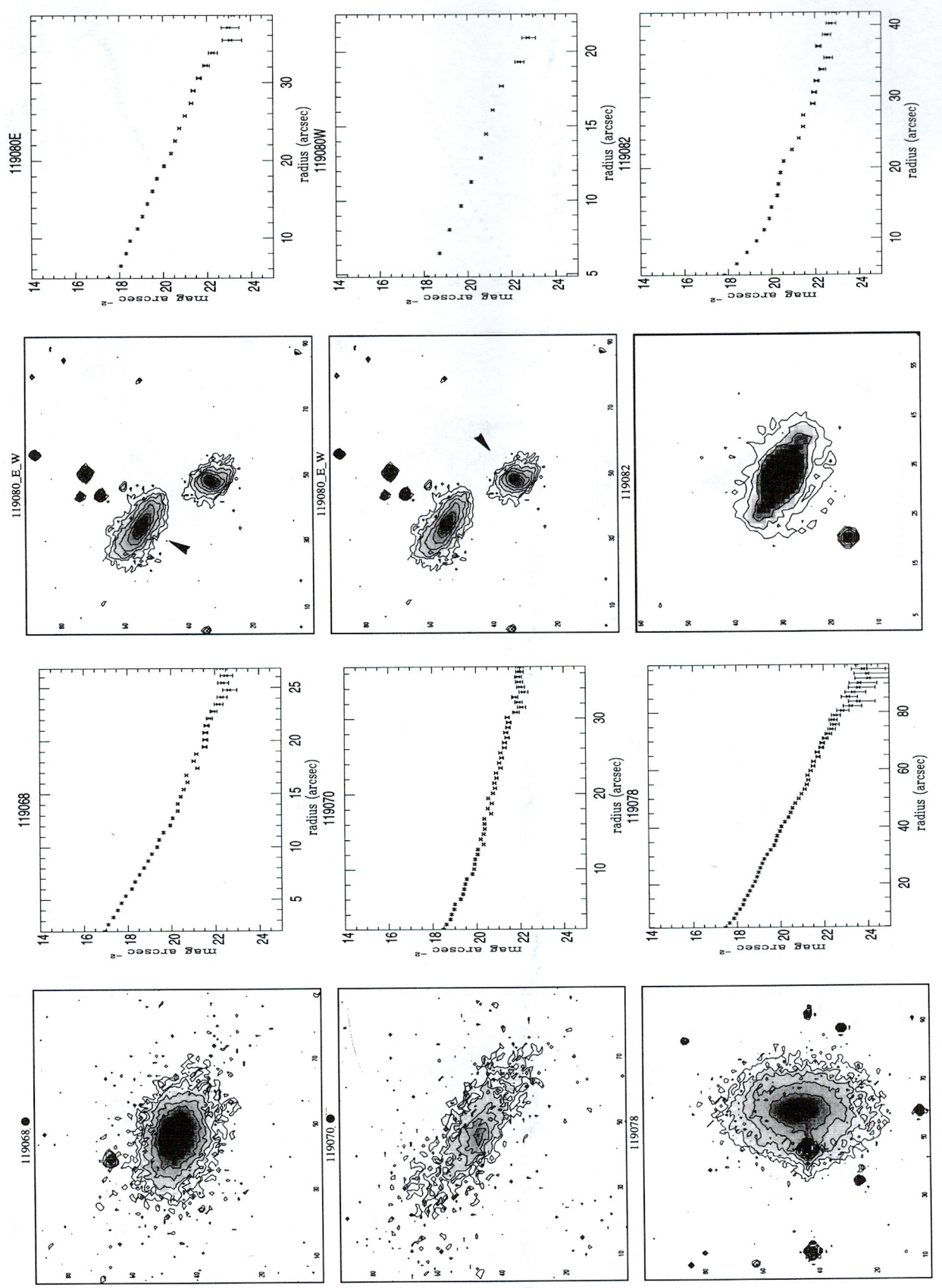

Fig. 1. continued. **(To be seen in landscape)**

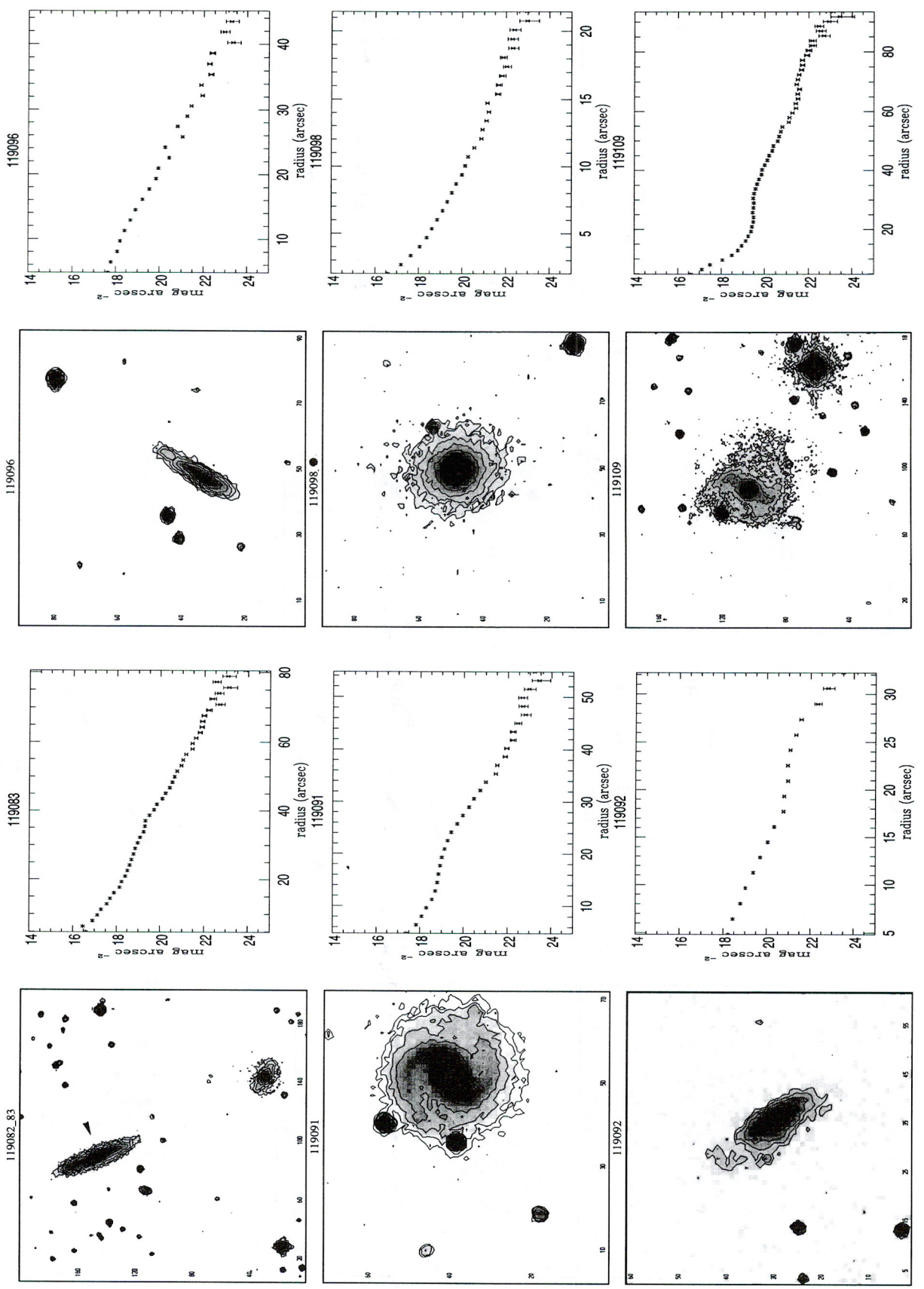

Fig. 1. continued. **(To be seen in landscape)**

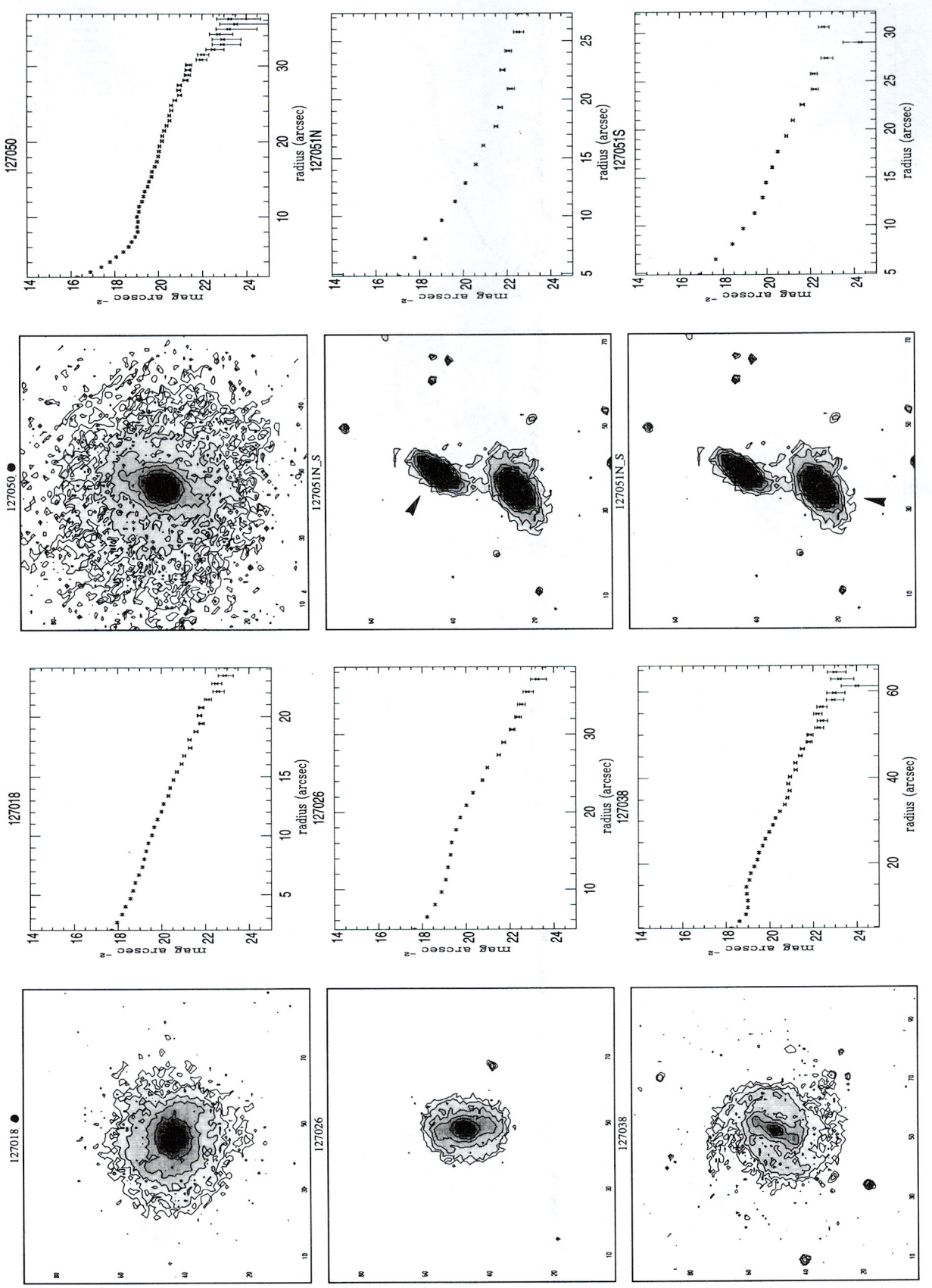

Fig. 1. continued. **(To be seen in landscape)**

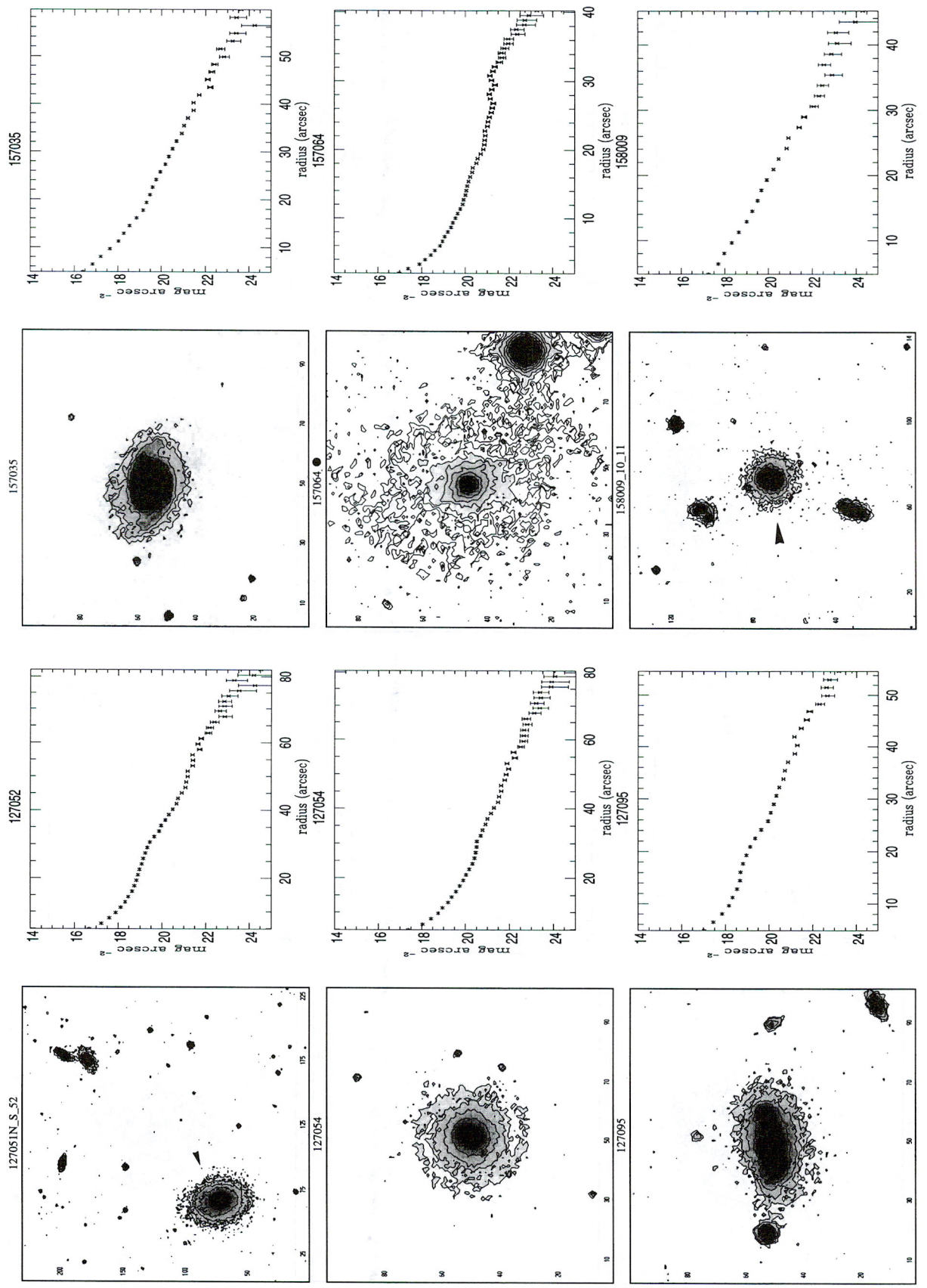

Fig. 1. continued. **(To be seen in landscape)**

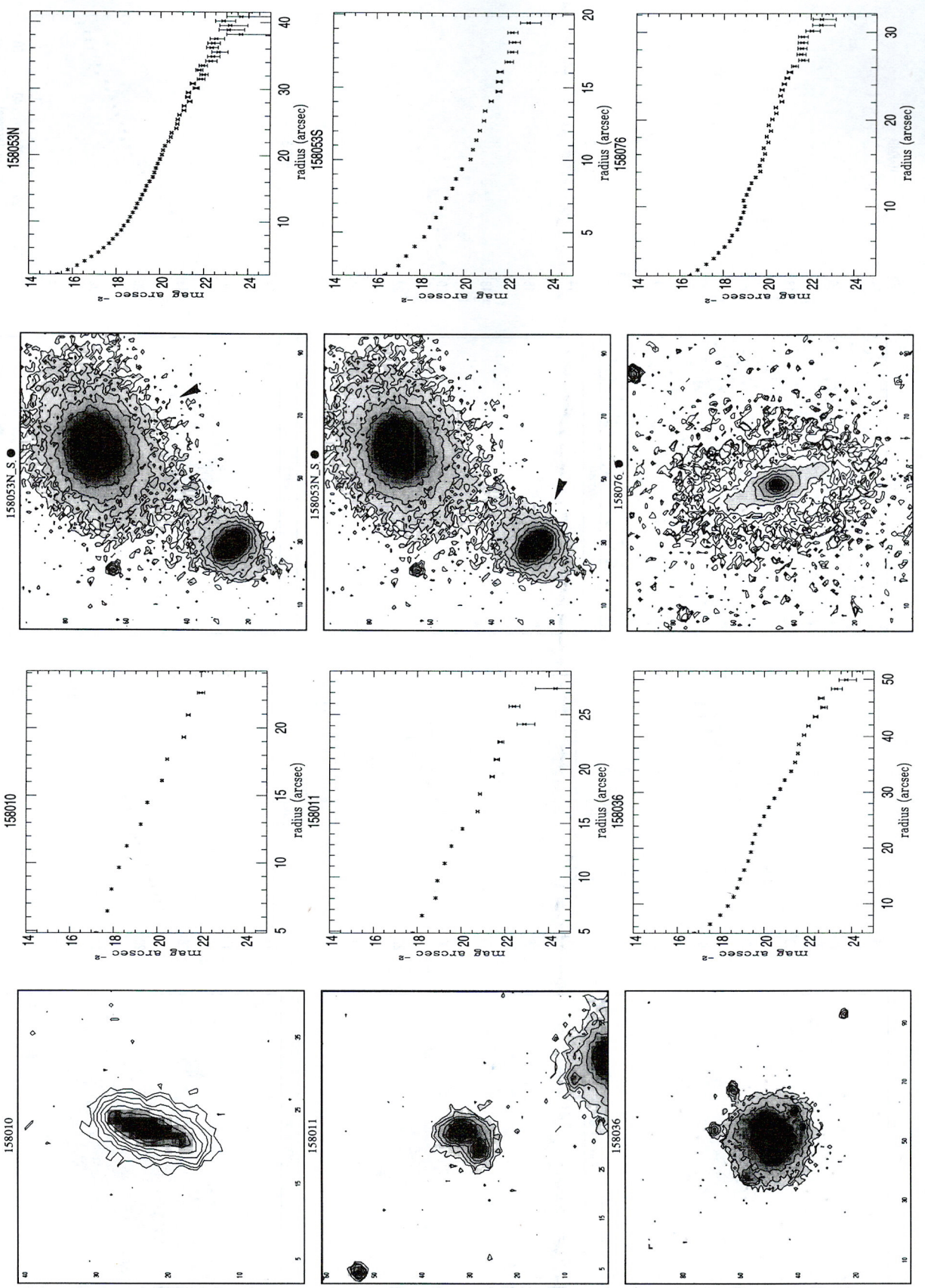

Fig. 1. continued. **(To be seen in landscape)**

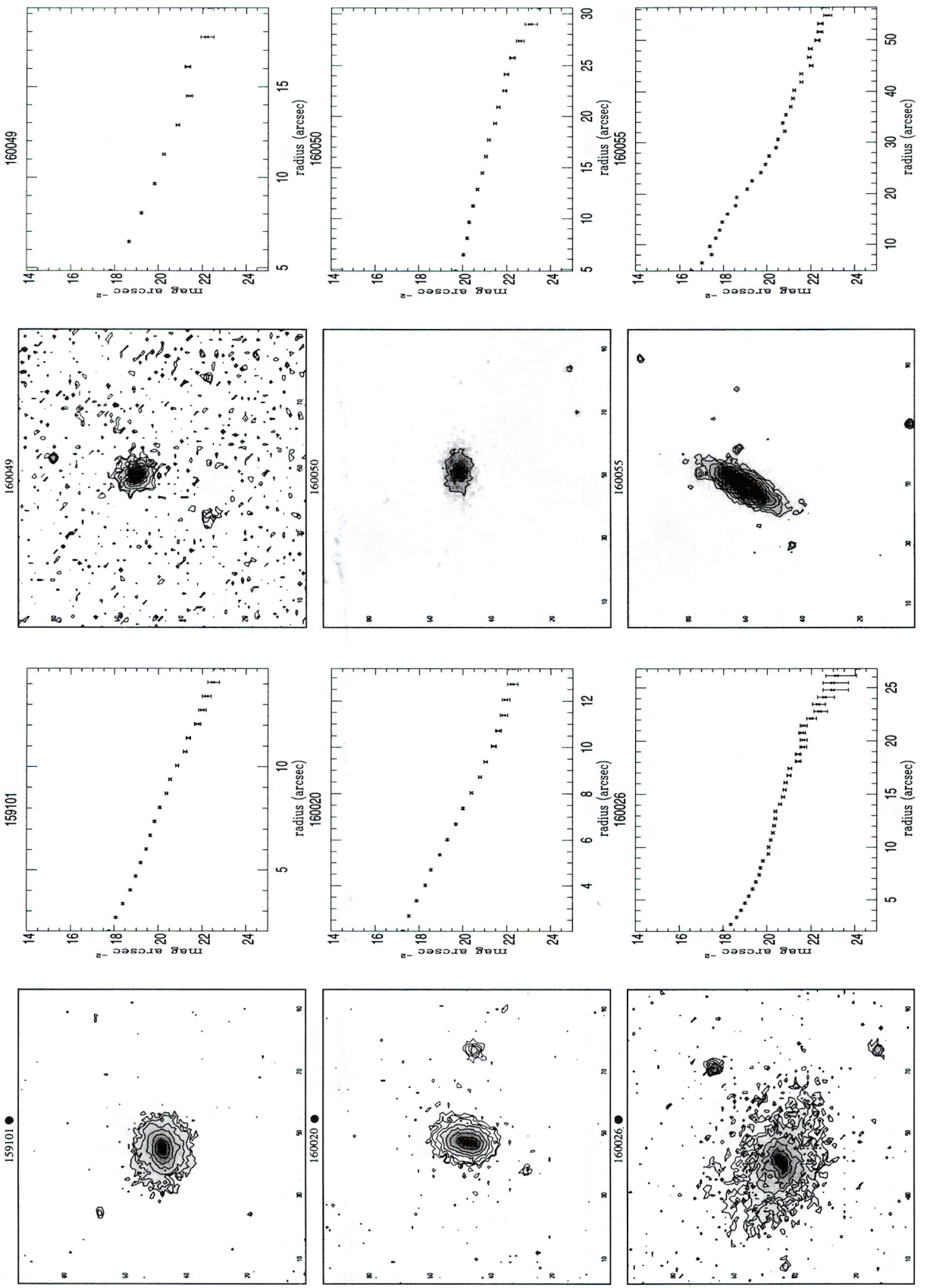

Fig. 1. continued. **(To be seen in landscape)**

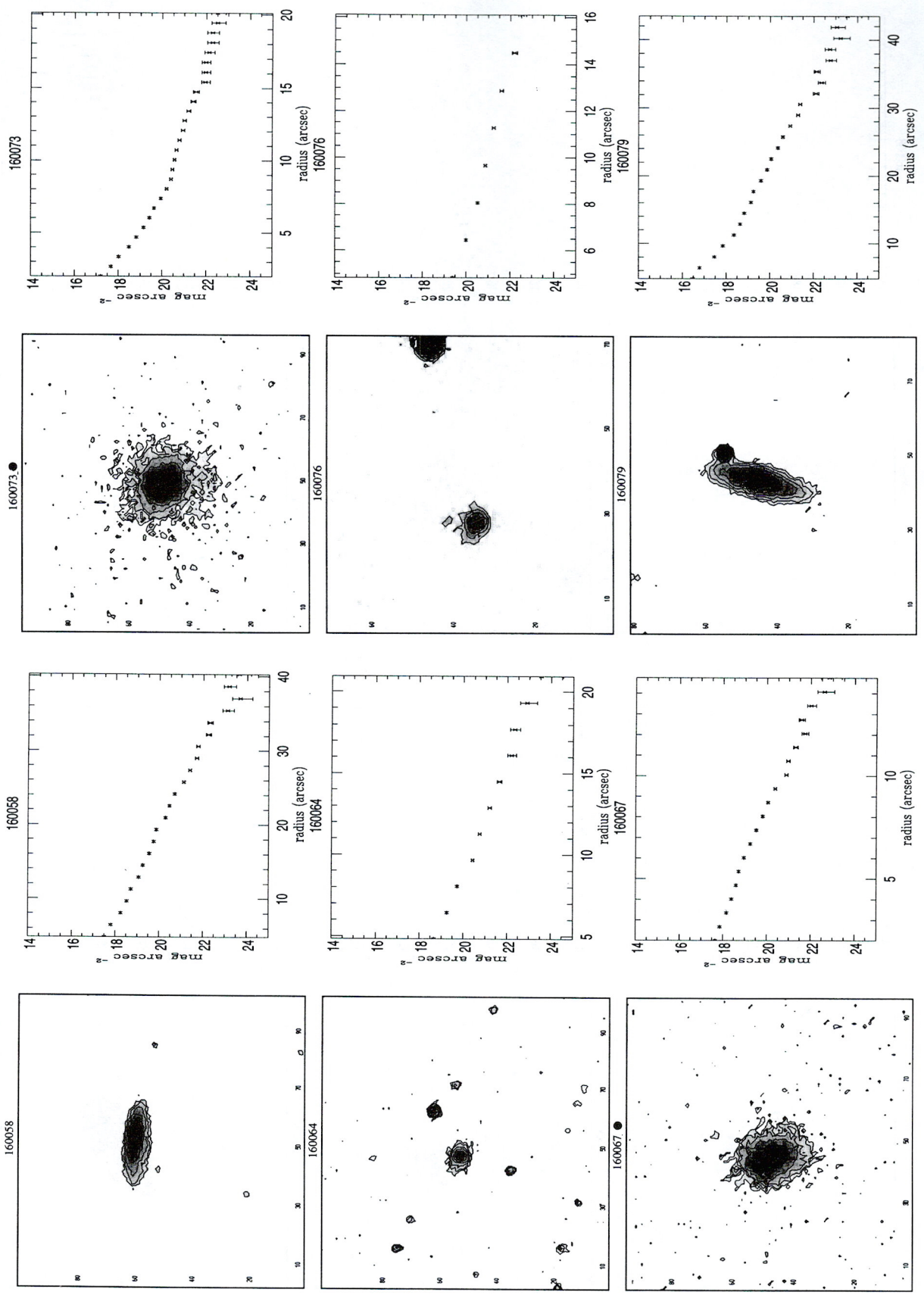

Fig. 1. continued. **(To be seen in landscape)**

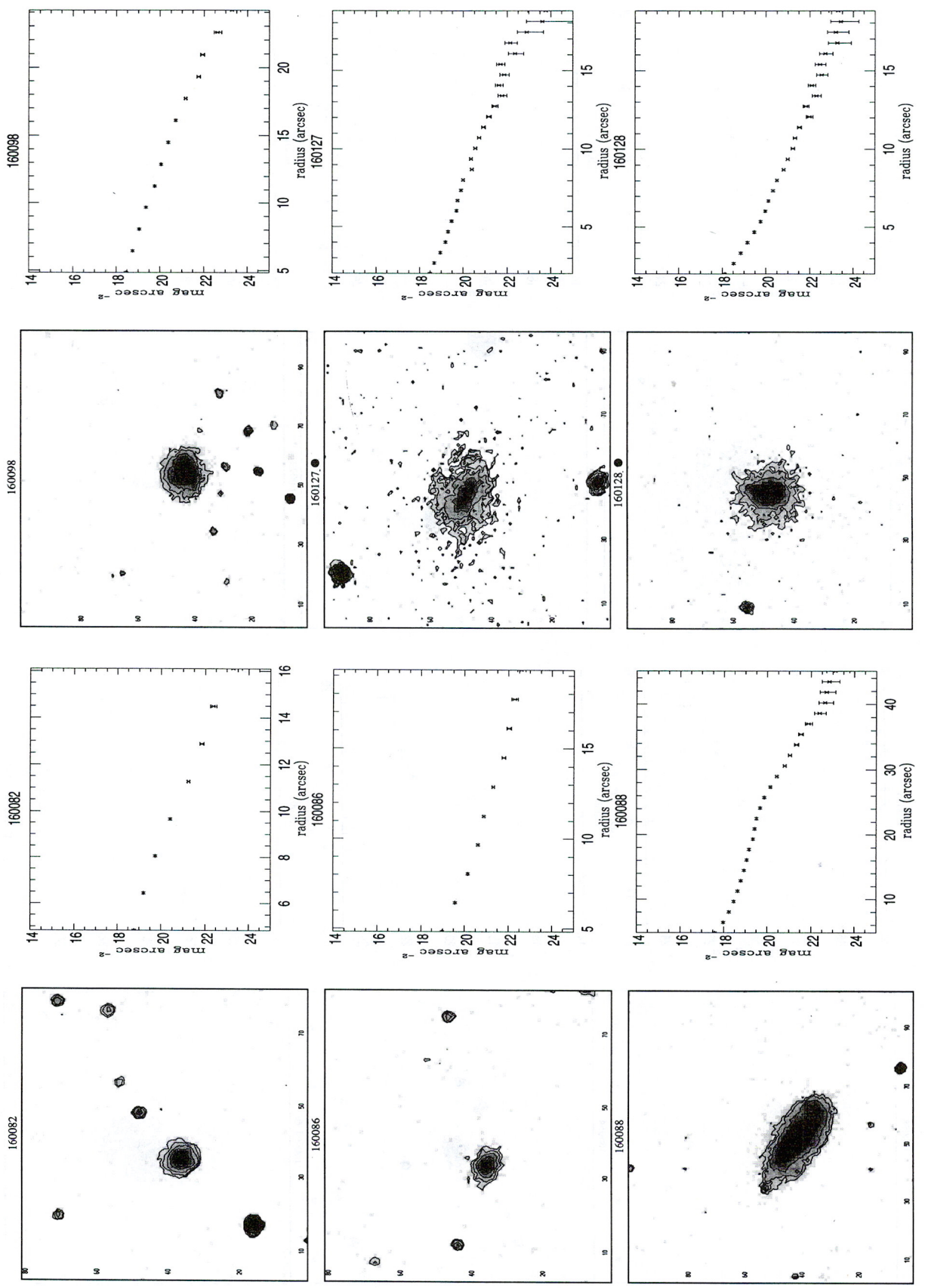

Fig. 1. continued. **(To be seen in landscape)**

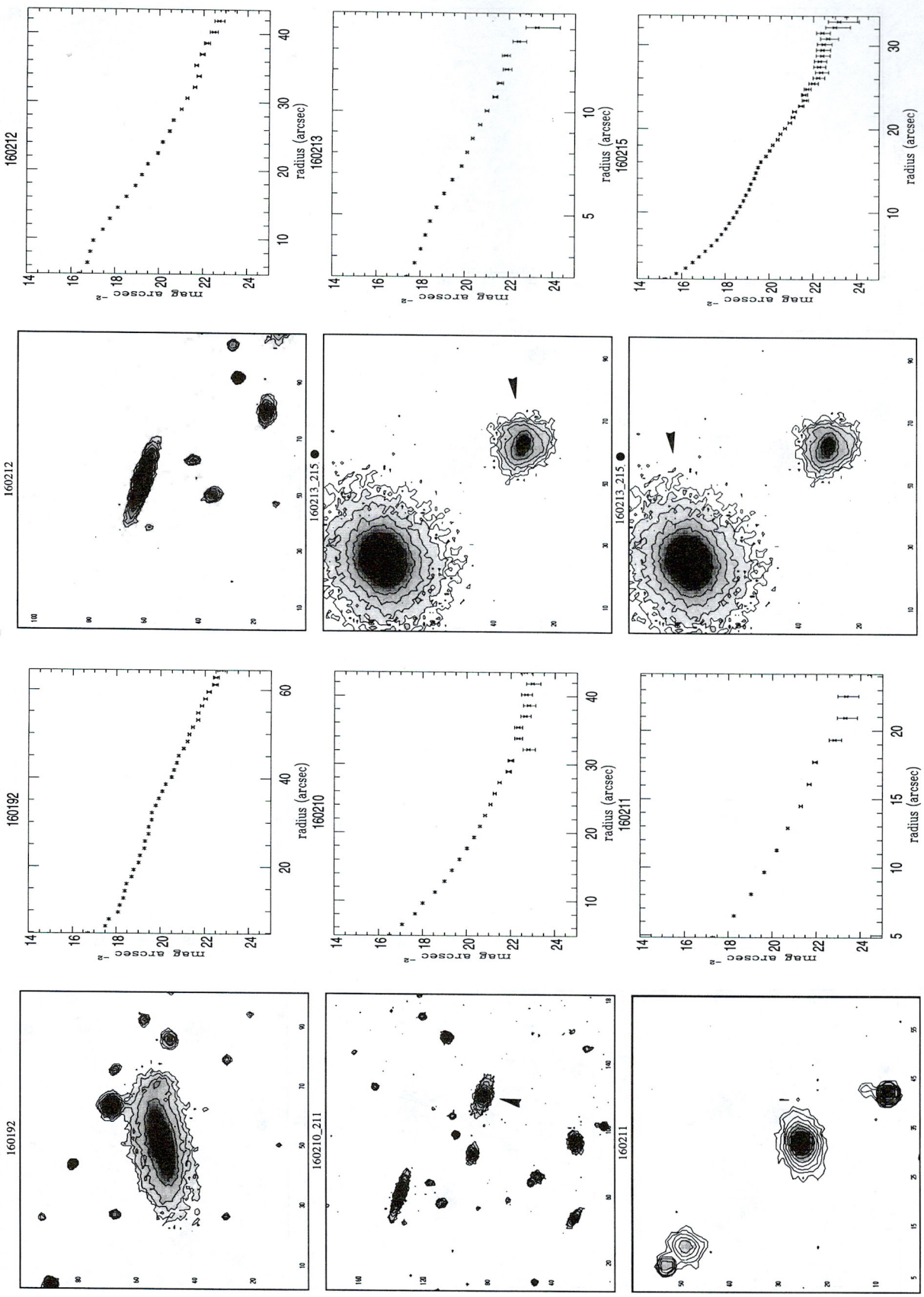

Fig. 1. continued. **(To be seen in landscape)**

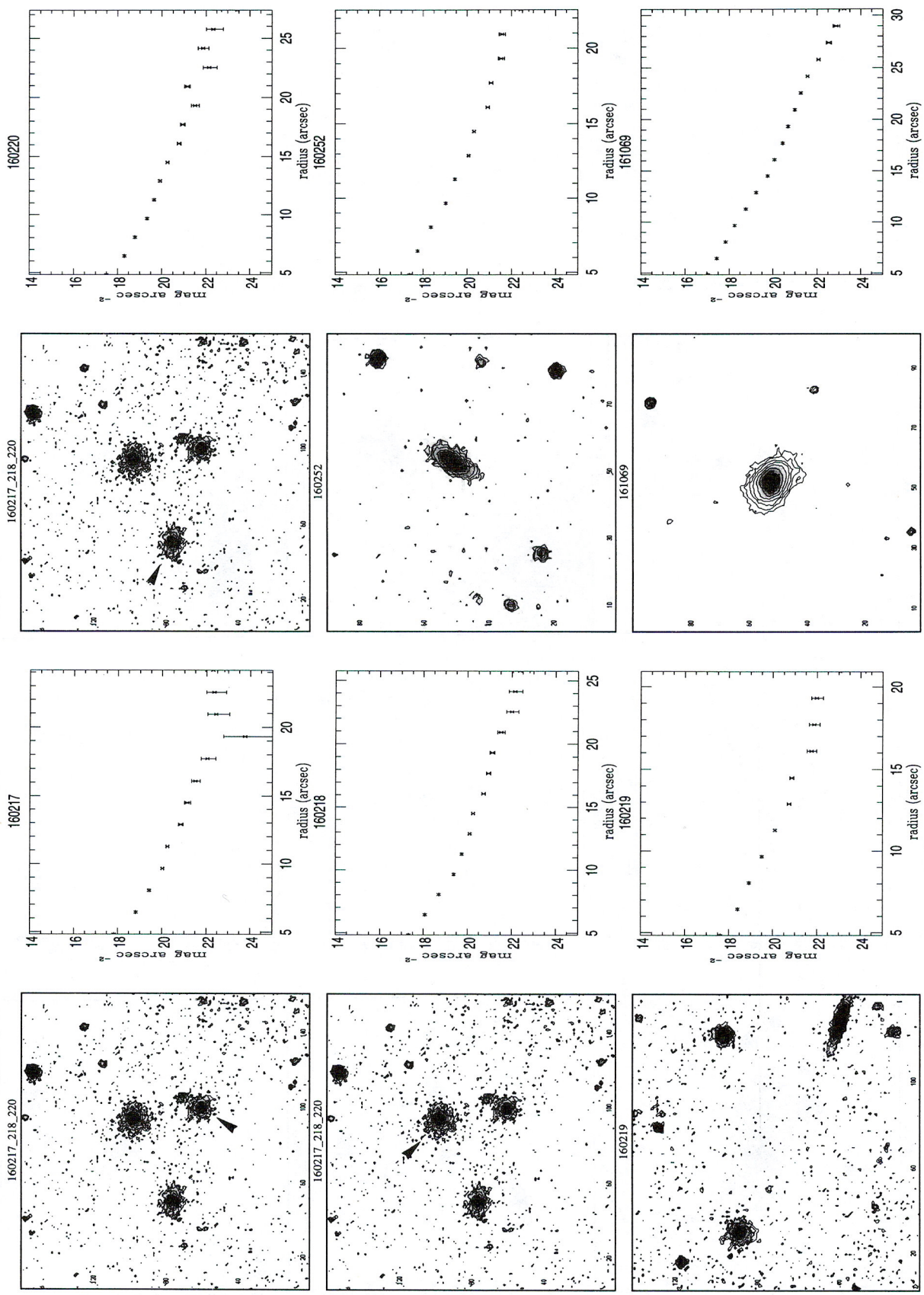

Fig. 1. continued. **(To be seen in landscape)**

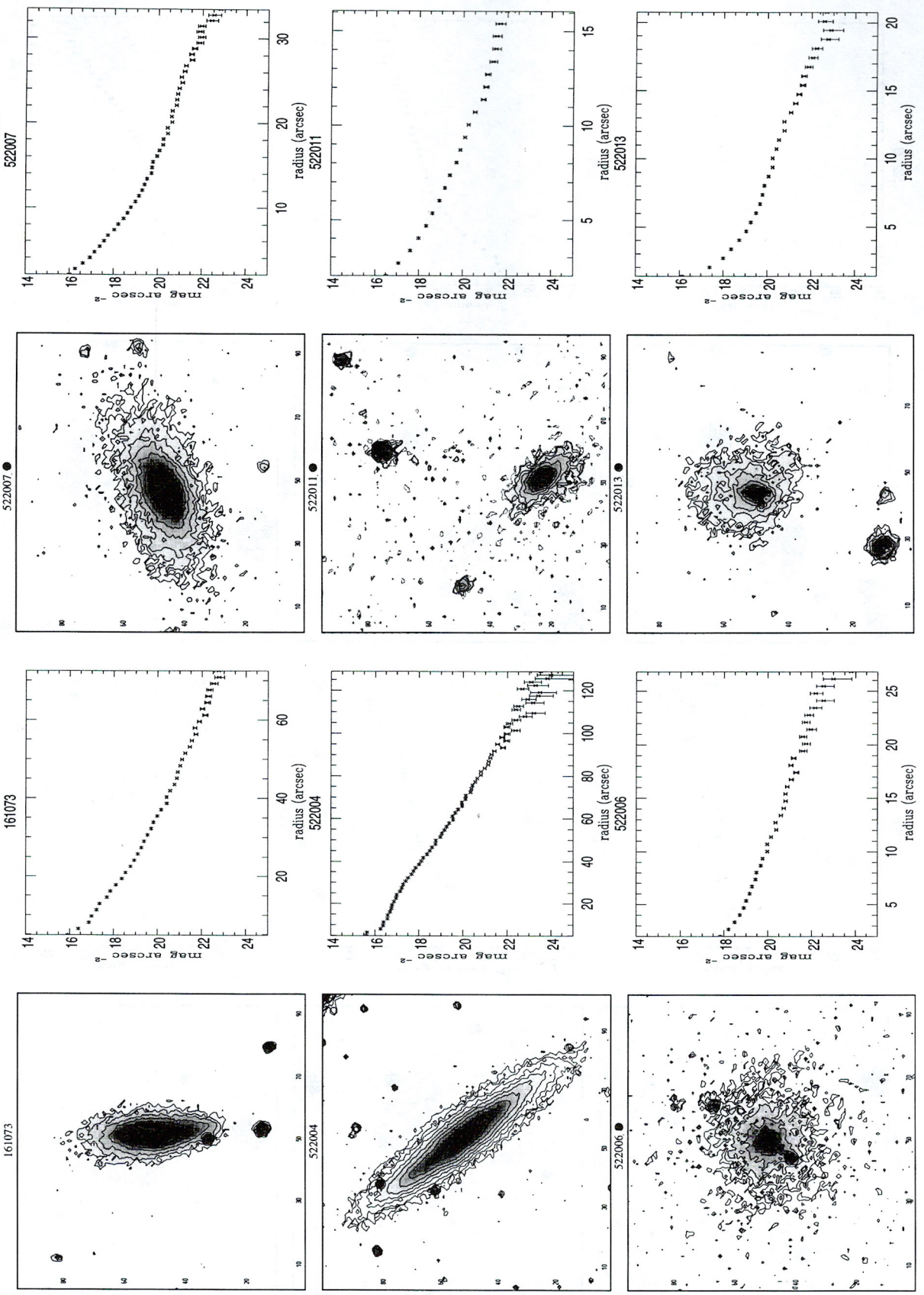

Fig. 1. continued. **(To be seen in landscape)**

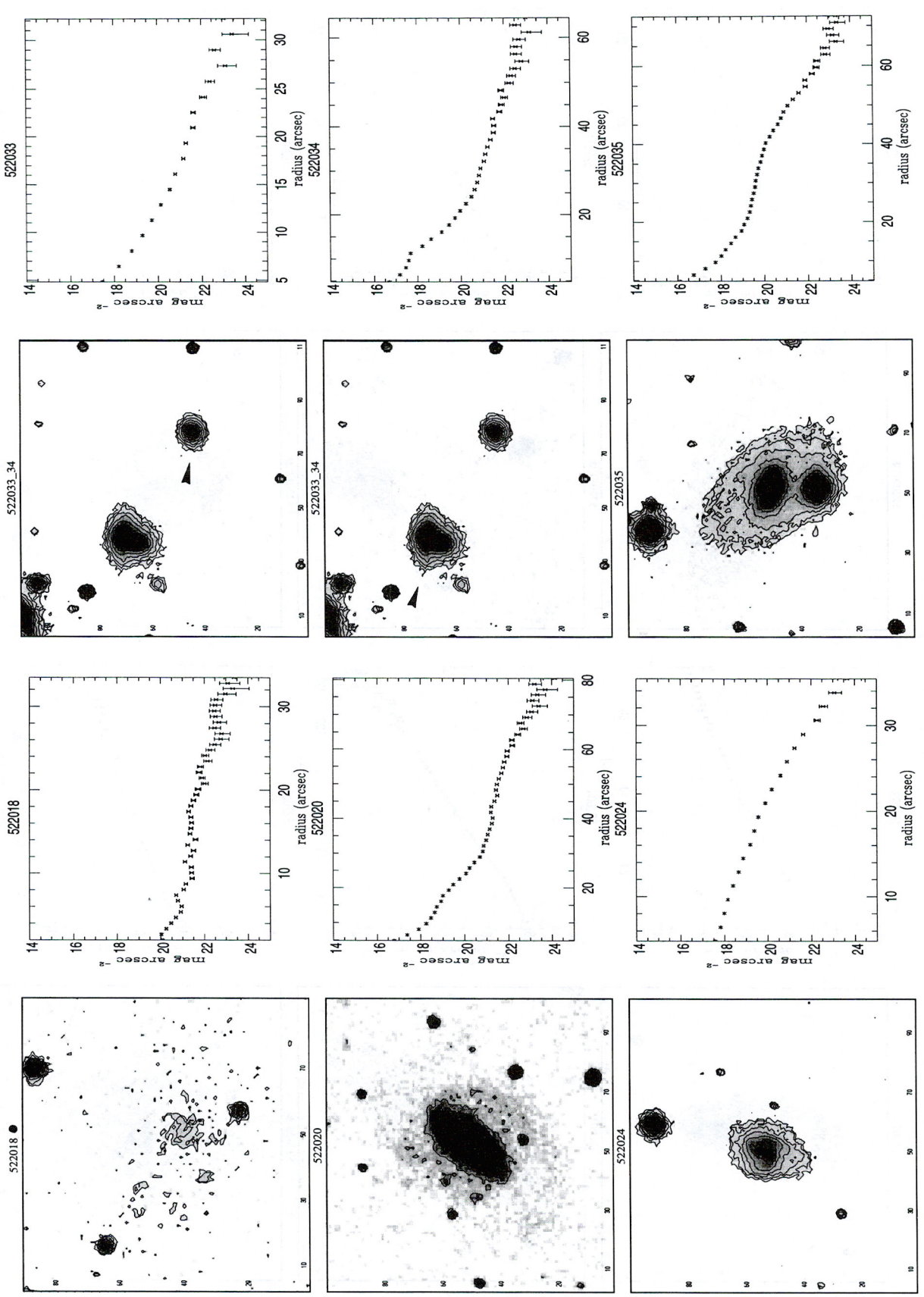

Fig. 1. continued. **(To be seen in landscape)**

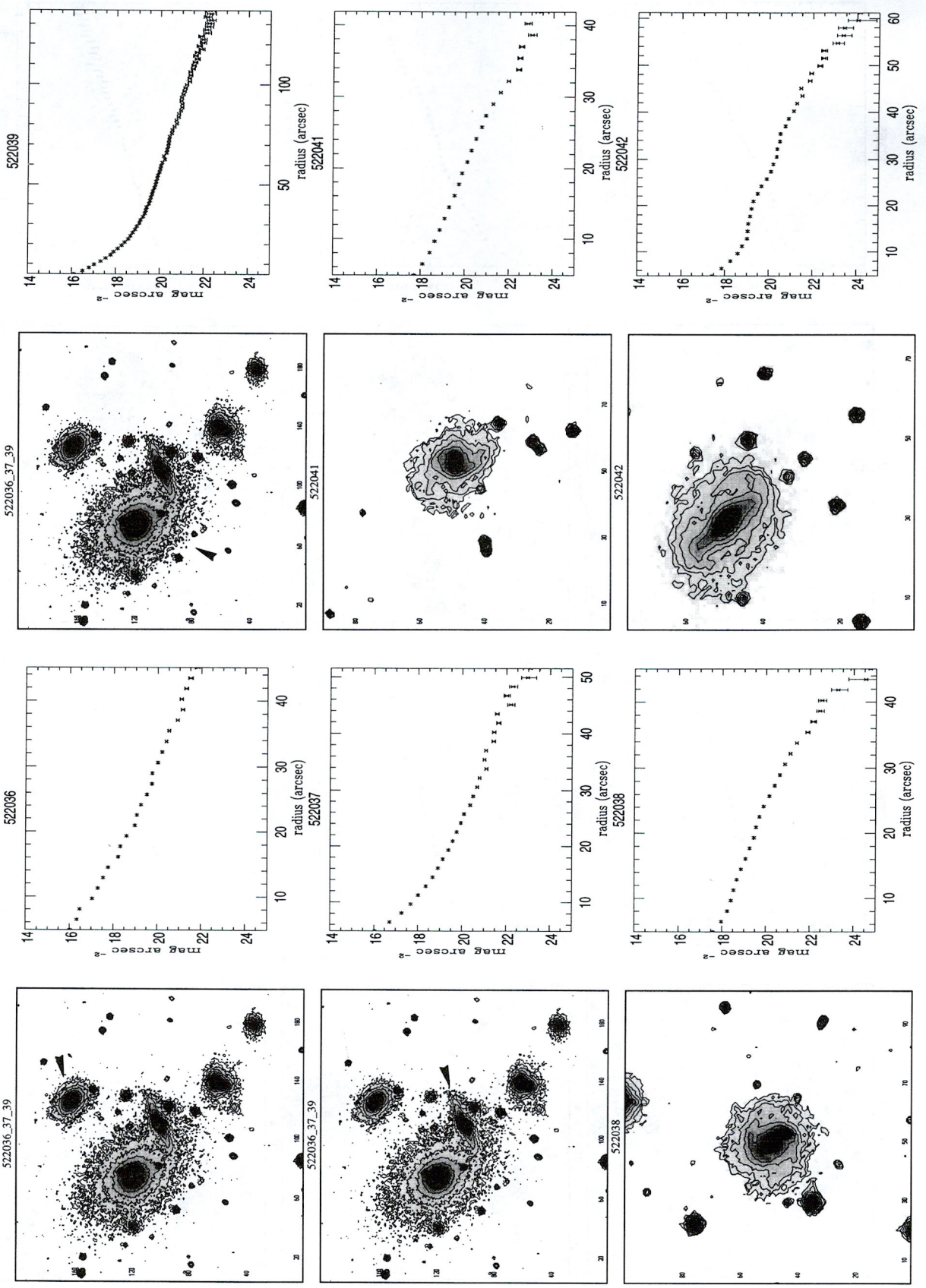

Fig. 1. continued. **(To be seen in landscape)**

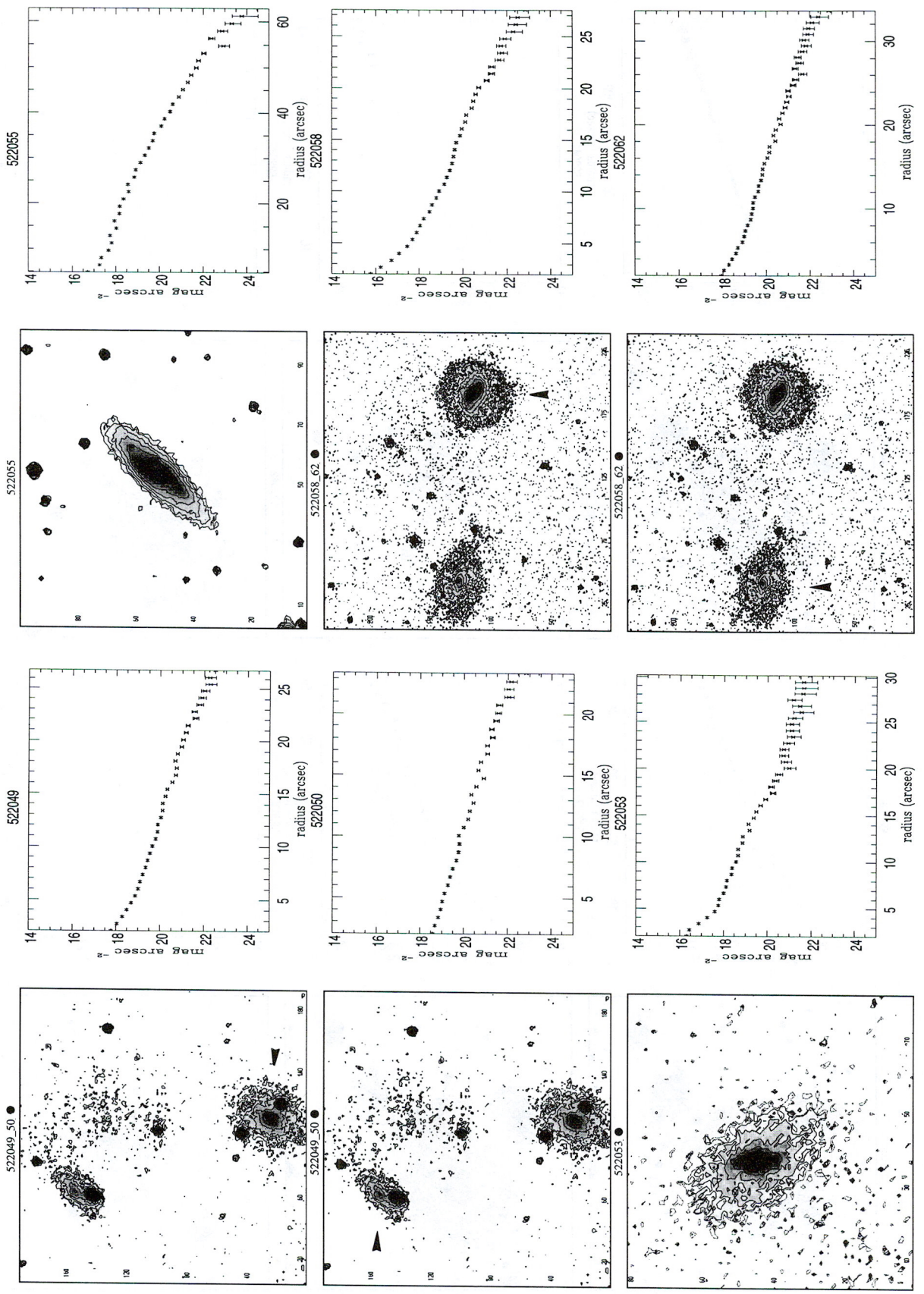

Fig. 1. continued. **(To be seen in landscape)**

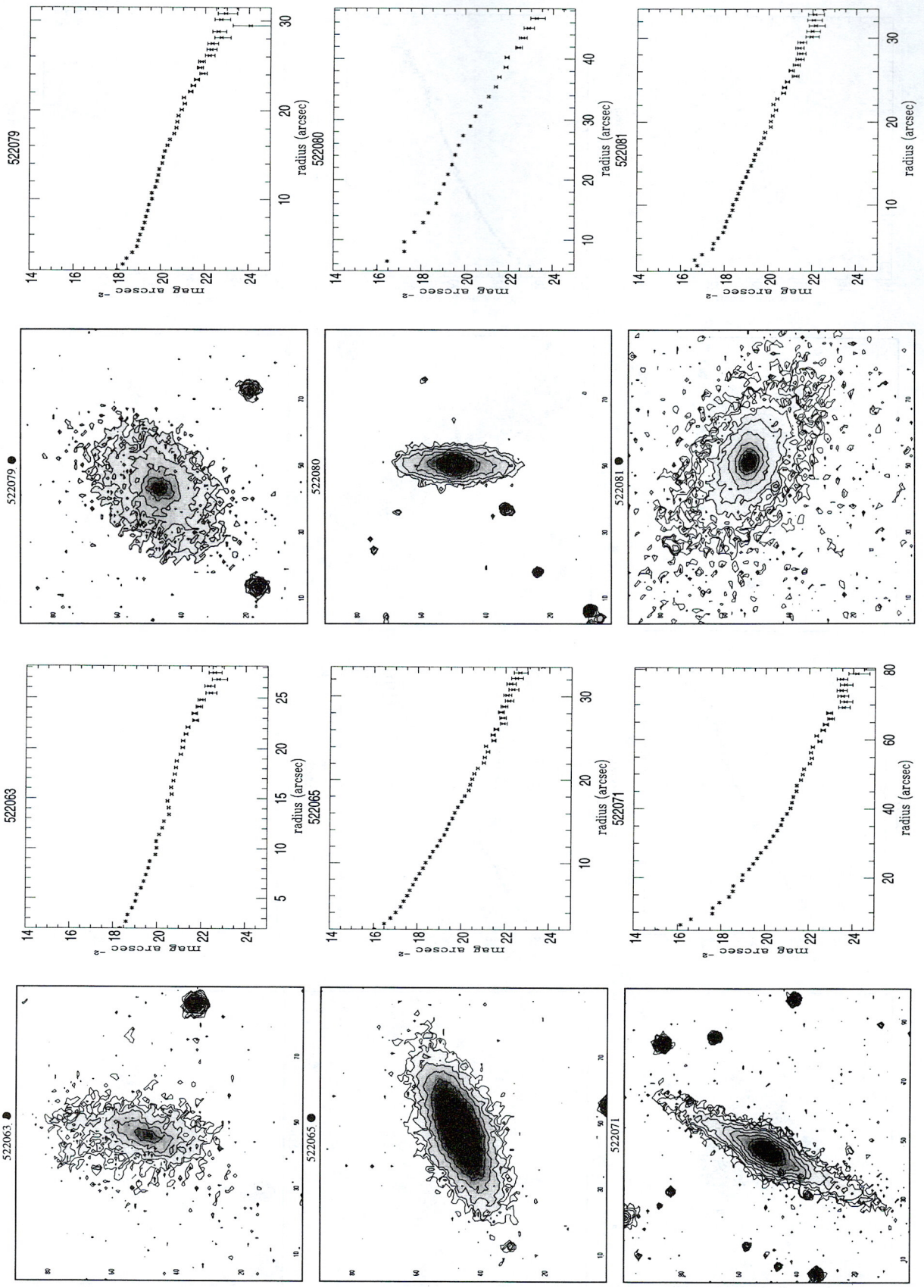

Fig. 1. continued. **(To be seen in landscape)**

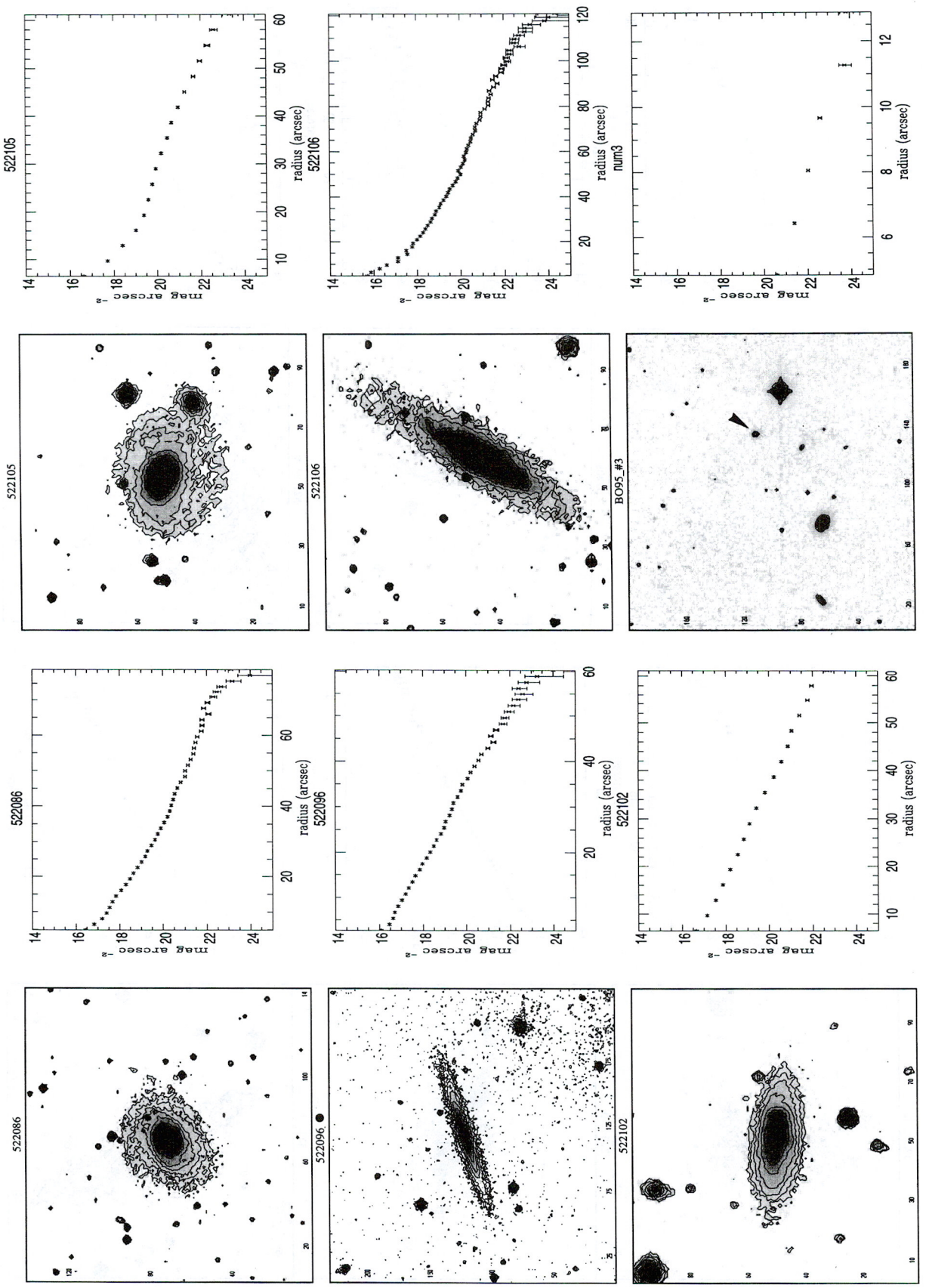

Fig. 1. continued. **(To be seen in landscape)**

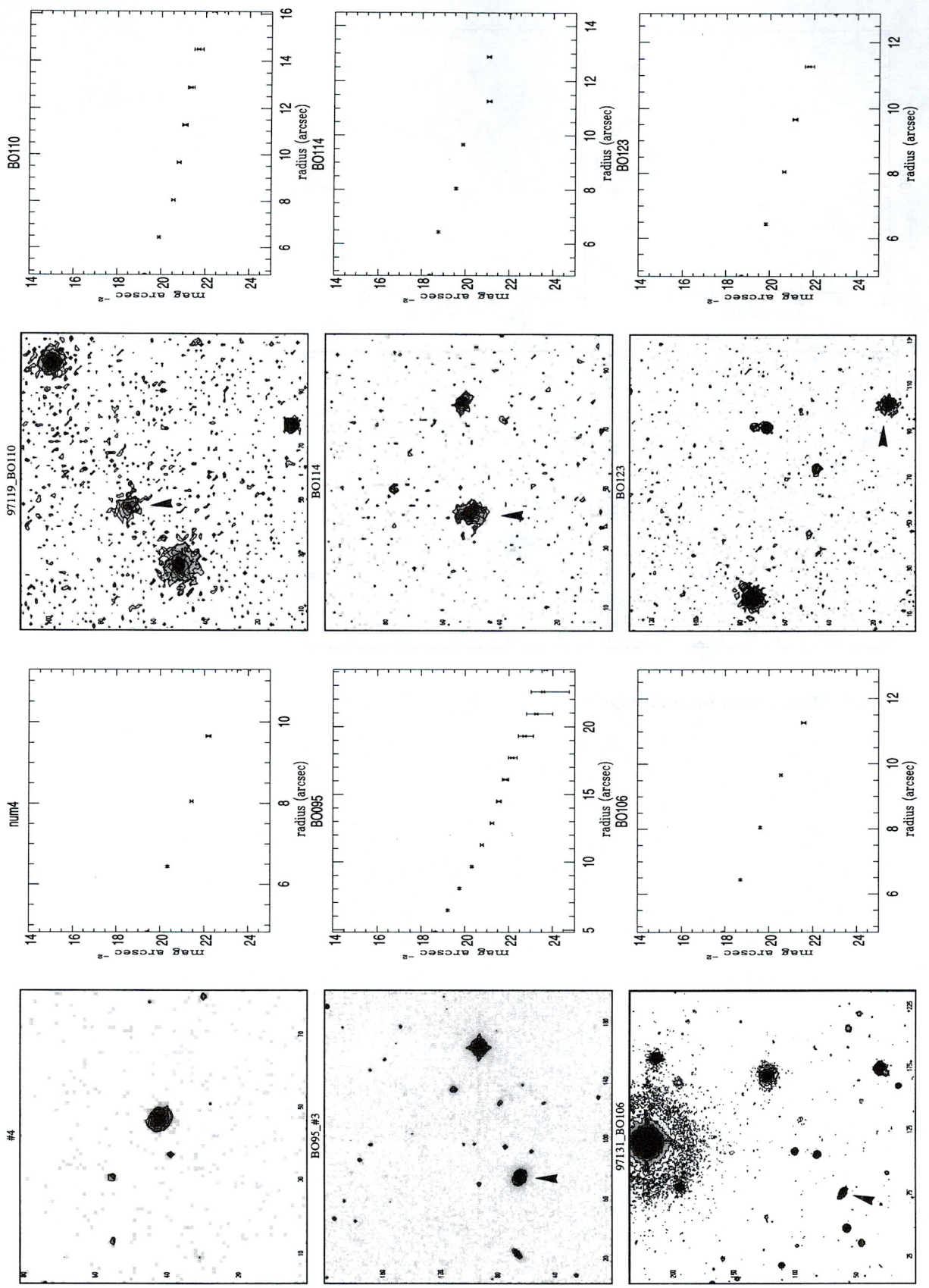

Fig. 1. continued. **(To be seen in landscape)**

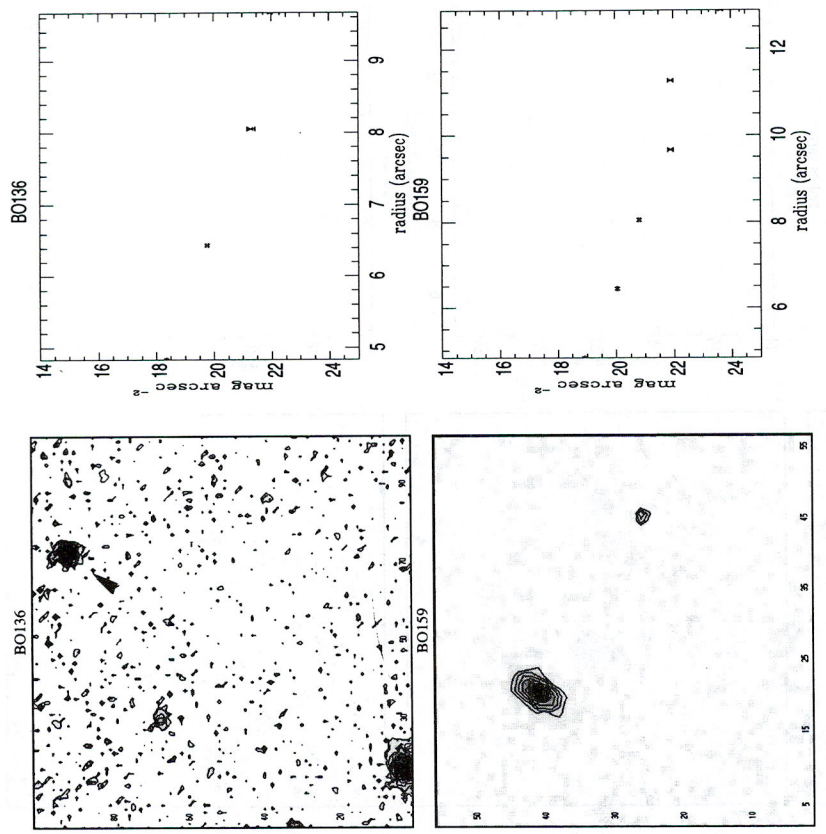

Fig. 1. continued. **(To be seen in landscape)**